TECHNICAL REPORT RD-MG-97-6

SYNTHETIC APERTURE RADAR SYSTEM PROCESSING WITH A NONUNIFORM PULSE REPETITION INTERVAL

Stacie Mobley
Missile Guidance Directorate
Missile Research, Development, and Engineering Center

March 1997

Approved for public release; distribution is unlimited.

DESTRUCTION NOTICE

FOR CLASSIFIED DOCUMENTS, FOLLOW THE PROCEDURES IN DoD 5200.22-M, INDUSTRIAL SECURITY MANUAL, SECTION II-19 OR DoD 5200.1-R, INFORMATION SECURITY PROGRAM REGULATION, CHAPTER IX. FOR UNCLASSIFIED, LIMITED DOCUMENTS, DESTROY BY ANY METHOD THAT WILL PREVENT DISCLOSURE OF CONTENTS OR RECONSTRUCTION OF THE DOCUMENT.

DISCLAIMER

THE FINDINGS IN THIS REPORT ARE NOT TO BE CONSTRUED AS AN OFFICIAL DEPARTMENT OF THE ARMY POSITION UNLESS SO DESIGNATED BY OTHER AUTHORIZED DOCUMENTS.

TRADE NAMES

USE OF TRADE NAMES OR MANUFACTURERS IN THIS REPORT DOES NOT CONSTITUTE AN OFFICIAL ENDORSEMENT OR APPROVAL OF THE USE OF SUCH COMMERCIAL HARDWARE OR SOFTWARE.

REPORT DOCUMENTATION PAGE

Form Approved
OMB No. 0704-0188

1a. REPORT SECURITY CLASSIFICATION
UNCLASSIFIED

1b. RESTRICTIVE MARKINGS

2a. SECURITY CLASSIFICATION AUTHORITY

3. DISTRIBUTION ORGANIZATION REPORT NUMBER(S)
Approved for public release; distribution is unlimited.

2b. DECLASSIFICATION/DOWNGRADING SCHEDULE

4. PERFORMING ORGANIZATION REPORT NUMBER(S)
TR-RD-MG-97-6

5. MONITORING ORGANIZATION REPORT NUMBER(S)

6a. NAME OF PERFORMING ORGANIZATION
Missile Guidance Directorate
Res., Dev., and Eng. Ctr.

6b. OFFICE SYMBOL (If Applicable)
AMSMI-RD-MG-RF

7a. NAME OF MONITORING ORGANIZATION

6c. ADDRESS (City, State, and ZIP Code)
Commander, U. S. Army Missile Command
ATTN: AMSMI-RD-MG-RF
Redstone Arsenal, AL 35898

7b. ADDRESS (City, State, and ZIP Code)

8a. NAME OF FUNDING/SPONSORING ORGANIZATION

8b. OFFICE SYMBOL (If Applicable)

9. PROCUREMENT INSTRUMENT IDENTIFICATION NUMBER

8c. ADDRESS (City, State, and ZIP Code)

10. SOURCE OF FUNDING NUMBERS

PROGRAM ELEMENT NO.	PROJECT NO.	TASK NO.	WORK UNIT ACCESSION NO.

11. TITLE (Include Security Classification)
Synthetic Aperture Radar System Processing with a Nonuniform Pulse Repetition Interval

12. PERSONAL AUTHOR(S)
Stacie Mobley

13a. TYPE OF REPORT	13b. TIME COVERED	14. DATE OF REPORT (Year, Month, Day)	15. PAGE COUNT
Final	FROM Aug 93 TO Feb 95	March 1997	76

16. SUPPLEMENTARY NOTATION

17. COSATI CODES			18. SUBJECT TERMS (Continue on reverse if necessary and identify by block number)
FIELD	GROUP	SUB-GROUP	Synthetic Aperture Radar (SAR), Pulse Repetition Interval (PRI), Doppler, Side-Lobes

19. ABSTRACT (Continue on reverse if necessary and identify by block number)

Based on recent developments it has become feasible to combine the multiple pulse integration of Synthetic Aperture Radar (SAR) with the temporal agility of nonuniform Pulse Repetition Intervals (PRIs). This combination can bring to the traditional SAR system both strong resistance to countermeasures and interception, and high sensitivity. A significant problem which must be addressed in SAR systems is the possible smearing of the azimuth dimension of the image due to Doppler side-lobes which are too high. This issue is even more serious with a nonuniform PRI waveform. One method for increasing the side-lobe rejection capability of these waveforms is through the use of interpolation techniques. The improved performance obtained by this method is illustrated through the use of the two examples.

20. DISTRIBUTION/AVAILABILITY OF ABSTRACT
☐ UNCLASSIFIED/UNLIMITED ☒ SAME AS RPT. ☐ DTIC USERS

21. ABSTRACT SECURITY CLASSIFICATION
UNCLASSIFIED

22a. NAME OF RESPONSIBLE INDIVIDUAL
Stacie Mobley

22b. TELEPHONE (Include Area Code)
(205) 876-4817

22c. OFFICE SYMBOL
AMSMI-RD-MG-RF

DD Form 1473, JUN 86 *Previous editions are obsolete.*

SECURITY CLASSIFICATION OF THIS PAGE
UNCLASSIFIED

TABLE OF CONTENTS

	Page
I. INTRODUCTION	1
II. HISTORY OF SAR	2
III. THEORY OF SAR	5
A. Variations of SAR	5
B. Real Beam Radar Considerations	7
C. SAR Basics	10
IV. THEORY RELATED TO NONUNIFORM PRI	24
A. Definition of Nonuniform PRI	24
B. Waveform Processing Concepts	24
C. Interpolation Method for Processing Nonuniform Pulse Trains	25
V. ANALYSIS AND RESULTS OF INTERPOLATION BASED APPROACH	27
VI. INTERPRETATION OF RESULTS	47
VII. CONCLUSIONS	53
REFERENCES	55
LIST OF SYMBOLS	57
APPENDIX A: PARAMETERS FOR SCENARIO A	A-1
APPENDIX B: PARAMETERS FOR SCENARIO B	B-1

LIST OF ILLUSTRATIONS

Figure	Title	Page
1.	Side-Looking SAR [7]	6
2.	Spotlight SAR [7]	7
3.	DBS [8]	7
4.	Resolution in the X-Direction [6]	8
5.	Geometry of a Real Array Imaging Radar [6]	10
6.	Transmitted and Received Signals from a Target [6]	11
7.	Frequency Spectrum of a Limited Duration Sinewave [6]	13
8.	Resolution Element D/2 in the Y-Direction [6]	13
9.	Range to a Point on the Ground as the Platform Flies with Velocity, V [6]	15
10.	Phase and Frequency Excursion of a Single Point on the Ground as a Function of Time [6]	17
11.	Platform Flight and Frequency History of Points on the Ground [6]	18
12.	Range Gates Followed by Doppler Filters for Electronic Data Processing	19
13.	Maximum and Minimum Range-to-Ground for the 3dB Antenna Beamwidth, Q_{BW} [6]	20
14.	Ground Coverage in the Y-Direction for a 3 dB Beamwidth, Q_{BW} [6]	21
15.	Transmitted Pulse and Spectral Diagram of PRF Lines [6]	22
16.	Antenna Radiation Pattern for a 6-Inch Circular Antenna at 35 GHz	28
17.	Antenna Radiation Pattern for a 24-Inch Circular Antenna at 10 GHz	29
18.	Frequency Response for a Uniform PRF of 55 kHz	30
19.	Product of Response and Antenna Pattern for Uniform PRF of 55 kHz	30
20.	Frequency Response for $\pm$5 Percent Random Variation of PRF About 55 kHz.	31

LIST OF ILLUSTRATIONS (cont.)

Figure	Title	Page
21.	Product of Response and Antenna Pattern for ±5 Percent Random Variation About a PRF of 55 kHz	31
22.	Frequency Response of Widely Random Variation of PRF About 55 kHz	32
23.	Product of Response and Antenna Pattern for Widely Random Variation of PRF About 55 kHz	32
24.	Frequency Response of Interpolation for the ±5 Percent Random Variation with W = 20 kHz	33
25.	Product of Response and Antenna Pattern for Interpolation of ±5 Percent Random Variation with W = 20 kHz	33
26.	Frequency Response of Interpolation for ±5 Percent Random Variation About 55 kHz with W = 30 kHz	34
27.	Product of Response and Antenna Pattern for ±5 Percent Random Variation Interpolation with W = 30 kHz	34
28.	Frequency Response of Interpolation with Widely Random Variation and W = 20 kHz	35
29.	Product of Response and Antenna Pattern for Interpolation with Widely Random Variation and W = 20 kHz	35
30.	Frequency Response of Interpolation with Widely Random Variation and W = 30 kHz	36
31.	Product of Response and Antenna Pattern for Interpolation with Widely Random Variation and W = 30 kHz	36
32.	Monte Carloed Frequency Response of Interpolation with ±5 Percent Variation and W = 30 kHz	37
33.	Product of Monte Carloed Response and Antenna Pattern of Interpolation with ±5 Percent Variation and W = 30 kHz	37
34.	Frequency Response of Uniform PRF of 7.7 kHz	38
35.	Product of Response and Antenna Pattern for a Uniform PRF of 7.7 kHz	38

LIST OF ILLUSTRATIONS (cont.)

Figure	Title	Page
36.	Frequency Response for ±5 Percent Random Variation of PRF about 7.7 kHz.	39
37.	Product of Response and Antenna Pattern for ±5 Percent Random Variation About a PRF of 7.7 kHz	39
38.	Frequency Response of Widely Random Variation of PRF About 7.7 kHz	40
39.	Product of Response and Antenna Pattern for Widely Random Variation of PRF About 7.7 kHz	40
40.	Frequency Response of Interpolation for the ±5 Percent Random Variation with W = 3 kHz	41
41.	Product of Response and Antenna Pattern for Interpolation of ±5 Percent Random Variation with W = 3 kHz	41
42.	Frequency Response for Interpolation for ±5 Percent Random Variation About 7.7 kHz with W = 5 kHz	42
43.	Product of Response and Antenna Pattern for Interpolation of ±5 Percent Random Variation with W = 5 kHz	42
44.	Frequency Response of Interpolation with Widely Random Variation and W = 3 kHz	43
45.	Product of Response and Antenna Pattern for Interpolation of Widely Random Variation and W = 3 kHz	43
46.	Frequency Response of Interpolation with Widely Random Variation and W = 5 kHz	44
47.	Product of Response and Antenna Pattern for Interpolation with Widely Random Variation and W = 5 kHz	44
48.	Monte Carloed Frequency Response of Interpolation with ±5 Percent Variation about 7.7 kHz and W = 5 kHz	45
49.	Product of Monte Carloed Response and Antenna Pattern of Interpolation with ±5 Percent Variation and W = 5 kHz	45
50.	Antenna Pattern and Frequency Responses for Scenario A with ±5 Percent Random Variation	47

LIST OF ILLUSTRATIONS (conc.)

Figure	Title	Page
51.	Antenna Pattern and Frequency Responses for Scenario A Worst Case Random Variation	48
52.	Antenna Pattern and Frequency Responses for Scenario B with ±5 Percent Random Variation	48
53.	Antenna Pattern and Frequency Responses for Scenario B Worst Case Random Variation	49
54.	Main Beam of Antenna Pattern and Corresponding Frequency Responses for Scenario A ±5 Percent Random Variation	49
55.	Main Beam of Antenna Pattern and Corresponding Frequency Responses for Scenario A Worst Case Random Variation	50
56.	Main Beam of Antenna Pattern and Corresponding Frequency Responses for Scenario B ±5 Percent Random Variation	50
57.	Main Beam of Antenna Pattern and Corresponding Frequency Responses for Scenario B Worst Case Random Variation	51

I. INTRODUCTION

It has become feasible to attempt to combine the multiple pulse integration of Synthetic Aperture Radar (SAR) with the temporal agility of nonuniform pulse repetition intervals, based on the recent development of theory related to nonuniform Pulse Repetition Intervals (PRIs) as they apply to pulse Doppler radars [1]. This combination could bring to the traditional SAR system the benefits of both strong resistance to countermeasures and interception, and high sensitivity. These properties are very important in designing radar systems for military scenarios in which both an imaging capability and a capability against electronic countermeasures is desired.

A nonuniform PRI radar waveform is one where the spacing between the transmission of adjacent pulses is variable with time. The variation can be either random, repeating or modulated deterministically. This type of waveform has traditionally been used in noncoherent pulse radars where pulse to pulse processing is entirely noncoherent. In conventional SAR systems, as in pulse Doppler radars, the returns are coherently integrated for tens to thousands of pulses, and traditionally use only uniform interpulse periods during a coherent integration period. Uniform spacing is used in conventional radars because of the lower complexity of the resulting Doppler processing and the ability to generate large clutter rejections with simple signal processing algorithms. Clutter rejection is not an issue for SAR systems; however, the side-lobe levels are a major issue when the quality of the images are considered. This report will examine the design and processing of SAR waveforms using nonuniform PRIs.

There are two primary reasons for the interest in nonuniform PRI's for a SAR: Nonuniform PRI waveforms can gain high sensitivity by coherent integration gain while maintaining the strong countermeasures resistance of noncoherent nonuniform PRI waveforms. Such waveforms are much more difficult to intercept and characterize than uniform PRI waveforms. A significant problem with nonuniform PRI waveforms in a SAR system is the possible smearing of the azimuth dimension of the image if the doppler side-lobes are to large. In a traditional SAR, with a uniform PRI waveform, the side-lobes are controlled with signal processing techniques such as amplitude weighting. However, these simpler techniques are not applicable to a nonuniform PRI waveform. To provide the side-lobe rejection capability required for a nonuniform PRI waveform requires the use of a processor that consists of time varying linear digital filters to furnish controllable side-lobe properties. One way to design such a filter is through the use of interpolation based techniques as are described in References 1 and 2. It will be shown that using these techniques that waveforms can be generated and processed which maintain good side-lobe performance over a frequency region which is sufficient for a SAR imaging system

To compare the performance of the different waveforms, there has to be a common parameter that can be compared. There are two measures that are often used to quantify the level of these side-lobes; the Peak Side-Lobe Level (PSL) and the Integrated Side-Lobe Level (ISL). The PSL is a measure of the ratio of energy in the peak response of the signal to the peak side-lobe response and is closely associated with the probability that a side-lobe appears in an adjacent filter [2]. The ISL, a measure of the total energy distributed among the side-lobes, is important in determining how the signal used in forming the image is distributed throughout the Doppler filter bank [3].

II. HISTORY OF SAR

Radar had long been used as a tool for the detection and tracking of targets such as aircraft and ships prior to the discovery of SAR in the early 1950s. In 1903 a German scientist, Christian Hulsmeyer, demonstrated a ship collision avoidance radar [4]. In 1922, during his acceptance speech for the IRE Medal of Honor, Marconi stated the value of radar for detection and tracking of ships. Most of the early work done on radars in the United States was conducted at the Naval Research Laboratory (NRL). In 1922, the first continuous wave radar system was demonstrated by A. H. Taylor and later patented. It was not until 1934, however, that the first airborne pulsed radar system was demonstrated by R. M. Page of NRL. In a parallel effort, radar systems for detection and tracking of aircraft were developed in both Great Britain and Germany during the early 1930s. By 1935, each of these countries had successfully demonstrated the capability to track aircraft using short pulse ranging measurements. The first operational radar system is generally credited as being built by Sir Robert Watson-Watt in 1937. This evolved into the Chain Home network. These stations were used throughout World War II to track aircraft across Europe.

Early in World War II, operational airborne radars were deployed by the United States, Germany, and Great Britain. The first systems, which operated at VHF frequencies, were used for detection of other aircraft and ships with mixed success. Following the war improvements in these systems came rapidly, in large part as a result of high frequency component technology development at the Massachusetts Institute of Technology (MIT) Radiation Laboratory.

In the early 1950s, engineers first recognized that, instead of rotating the antenna to scan the target area, it could be fixed to the fuselage of the aircraft. This configuration allowed for much longer apertures, hence, improved along-track resolution. The earlier versions of these Side-Looking Aperture Radar (SLAR) systems were primarily used for military reconnaissance purposes. These systems typically operated at relatively high frequencies compared to ground based radar systems, to achieve good along track resolution. Some systems that operated at frequencies as high as 35 GHz with pulse durations a small fraction of a microsecond, were capable of producing imagery at resolutions in the 10 to 20 m range. It was not until the mid 1960s that the first high resolution SLAR images were declassified and made available for scientific use.

It is generally agreed that the earliest statement describing the use of Doppler frequency analysis as applied to a coherent moving radar was put forth by Carl Wiley, of Goodyear Aircraft Corporation, in June 1951. Wiley noted that the reflections from two fixed targets at an angular separation relative to the velocity vector could be resolved by frequency analysis of the along-track spectrum. This characteristic permitted the azimuth resolution of the return echoes to be enhanced by separating the echoes into groups based on their Doppler shift. In his patent application, Wiley referred to his technique as Doppler Beam Sharpening (DBS) rather than SAR, as it is known today. His design is today referred to as a squint mode SAR.

The radar group at the Goodyear research facility pursued Wiley's beam sharpening concept and built the first airborne SAR system, flown aboard a DC-3 in 1953. This system, which operated at 930 MHz, used a Yagi antenna with a real aperture beamwidth of 100-degrees. The coherent video was filtered to extract the desired portion of the Doppler spectrum, weighting was applied to the baseband analog signal, and the resulting signal was summed in a storage tube to achieve a synthetic beamwidth of approximately 1-degree.

An independent and nearly parallel development of SAR was carried out by a group at the University of Illinois under the direction of C. W. Sherwin. This group was initially interested in developing techniques to detect moving targets, based on their Doppler characteristics, using incoherent airborne SLAR data. It was in 1952 that a member of the group, John Kovaly, recognized that variation in terrain height produced distinctive peaks that migrated across the azimuth frequency spectrum. He reported that these experimental observations could provide the basis for a new type of radar with improved angular resolution. It was also in 1952 that Sherwin first reported the concept of a fully focused array at each range bin by providing the proper phase corrections. Also, he put forth the concept of motion compensation based on phase corrections derived from platform accelerometer measurements, as applied to the received signal before storage. These ideas eventually evolved into development of a coherent X-band radar system. The first published article that included a focussed strip image was in a 1953 University of Illinois report. This system was designed to study sea surface characteristics as well as ship and submarine wakes.

The accomplishments of the Illinois group lead to the initiation of a much larger effort. The study was coordinated by the University of Michigan and was termed Project Wolverine. The study team was commissioned by the U. S. Army to develop a high performance combat surveillance radar. They developed a number of operational airborne SAR systems that routinely began producing strip maps by 1958. This group is also credited with developing the first operational motion compensation system, using a Doppler navigator to measure long term average drifts in conjunction with a gyro to correct for short term yawing of the aircraft. Perhaps the most important development by Cutrona's group is the on board optical recorder and ground optical correlator for converting the coherent SAR video signal into high resolution strip images.

To obtain real-time inflight viewing, electronic processing techniques were investigated in the early to mid 1960s. Film was still considered a memory possibility, with a flying spot scanner used to read off the video and provide an electrical signal. The most promising approach for electronic storage appeared to be a storage tube. For correlation, tapped delay lines or a mixer/crystal filter band approach were used. The problem was that film memory is not real-time, and that the storage tube lacks the dynamic range and stability.

The late 1960s brought the advent of digital memory [5]. The problem now was to get the wideband analog signal into digital form. High-speed Analog-To-Digital (A/D) converter technology developed in this same time period. Broadband A/D converter technology was reaching the point at which 100 MHz speed (5-foot range resolution) became commercially available. Suitable memory for real-time processing was now practicable. Mating of the digital memory with digital arithmetic provided for an all digital approach to achieving real-time SAR.

The next problem, then, was to implement motion compensation to isolate the real-time, digitally correlated SAR image for effects of aircraft motion. To be fully useful, the motion compensation should preserve the image from degradations, regardless of whether the aircraft motion is caused by weather disturbances or intentional maneuvering.

Development of the airborne digital minicomputer made it possible to mechanize motion compensation in an efficient and generalized manner, avoiding the limitations associated with special-purpose circuitry. The early 1970s, therefore, saw real-time, motion compensated SAR imagery provided by an all digital subsystem.

There were a number of other activities, in conjunction with the development of these early SAR systems, which advanced the state of the art in component technology [4]. The key difference between the real aperture SLAR system and the SAR is that SAR is a coherent system. A coherent system requires both the magnitude and the phase of the echo samples to be preserved, which implies that the system pulse to pulse phase must be stable. The high power magnetron, which was such an important development for the SLAR, could not be used directly in the SAR system since the starting phase of each pulse was random. Instead the early SAR systems used a coho stalo arrangement, where, for each magnetron pulse, the starting phase of the pulse was measured. This phase was retained in a phase locked intermediate frequency COHerent Oscillator (COHO), referenced to the STable Local Oscillator (STALO), which was then used to demodulate the received echo.

A key advance in SAR technology was the development of linear beam power amplifiers such as the klystron in 1939, followed shortly by the Traveling Wave Tube (TWT). These devices provided both the high peak power and phase stability required for SAR systems. The major advance in the TWT over the klystron is the bandwidth. The klystron's bandwidth is limited to only a few percent of the carrier frequency, while the TWT is capable of octave bandwidths. Many of today's airborne SAR systems, and some spaceborne systems requiring high peak power, still use TWT technology, although solid state power amplifiers are now used in many applications because of their increased reliability. Just as the solid state high power transistor technology matured through the 1970s and 1980s, the technology of Monolithic Microwave Integrated Circuit (MMIC) devices is moving toward the forefront in the 1990s and should become the standard in the next generation of spaceborne and airborne SAR systems.

III. THEORY OF SAR

In Synthetic Aperture and Imaging Radars the transmission and reception of electromagnetic signals are used to obtain a "photograph" of the ground below. As is well known when any type of image is considered the quality and clarity of the image is determined by the resolution obtained in each dimension, i.e., the x- and y-directions. The y-direction will be considered to be along the flight path, and the x-direction will be considered to be perpendicular to the flight path.

Imaging radars can be divided into two broad categories; real array and synthetic array [6]. Imaging radars (both real and synthetic array) obtain x-direction resolution by controlling the transmitted pulsewidth. Real array radars obtain the y-direction resolution by the antenna beamwidth. Since the antenna beamwidth in each direction is inversely proportional to its length in that direction, the y-direction resolution of real array imaging radars is obtained through the use of long antennas.

The desire to use regular size airborne antennas for ground mapping led to the invention of SAR. These radars use the transmitted pulselength for the x-direction resolution, similar to real array imaging radars. However, SARs use the incremental Doppler shift of adjacent points on the ground for resolution in the y-direction, rather than the antenna beamwidth, as in the case of real array imaging radars. Therefore, the effect in going from a real array to a synthetic array, which reduces the size of the antenna, is the increased complexity of Doppler signal processing required for the y-direction resolution.

A. Variations of SAR

SAR is an airborne radar mapping technique for generating high resolution maps of surface target areas and terrain [7]. SAR is used to obtain fine resolution in both slant range and cross range. Cross-range resolution refers to resolution transverse to the radar's Line-of-Sight (LOS). The term, slant range, refers to the LOS range. Resolution in the slant range direction of the radar is often obtained by coding the transmitted pulse, typically FM chirp coding. Cross-range resolution is obtained by coherently integrating echo energy reflected from the ground as the platform carrying the radar travels above and along the illuminated area to be mapped.

The term *synthetic aperture* refers to the distance that the radar travels during the time that reflectivity data are collected from a point to be resolved on the surface, which remains illuminated by the real antenna beam. There are basically three variations of SAR: (1) Side-looking, (2) Spotlight, and (3) DBS. The length of the synthetic aperture of a side looking SAR is the ground track distance over which coherent integration occurs. *Synthetic length* depends on antenna beamwidth and varies with range delay. *Synthetic aperture length* shrinks in the side-looking case for echoes arriving from points closer to the radar, and increases for echoes arriving from points farther from the radar. The effect for ideal processing is to produce constant cross-range resolution versus range. Maximum possible cross-range resolution is approximately equal to one half of the real aperture's cross-range dimension. Figure 1 illustrates a side-looking SAR configuration.

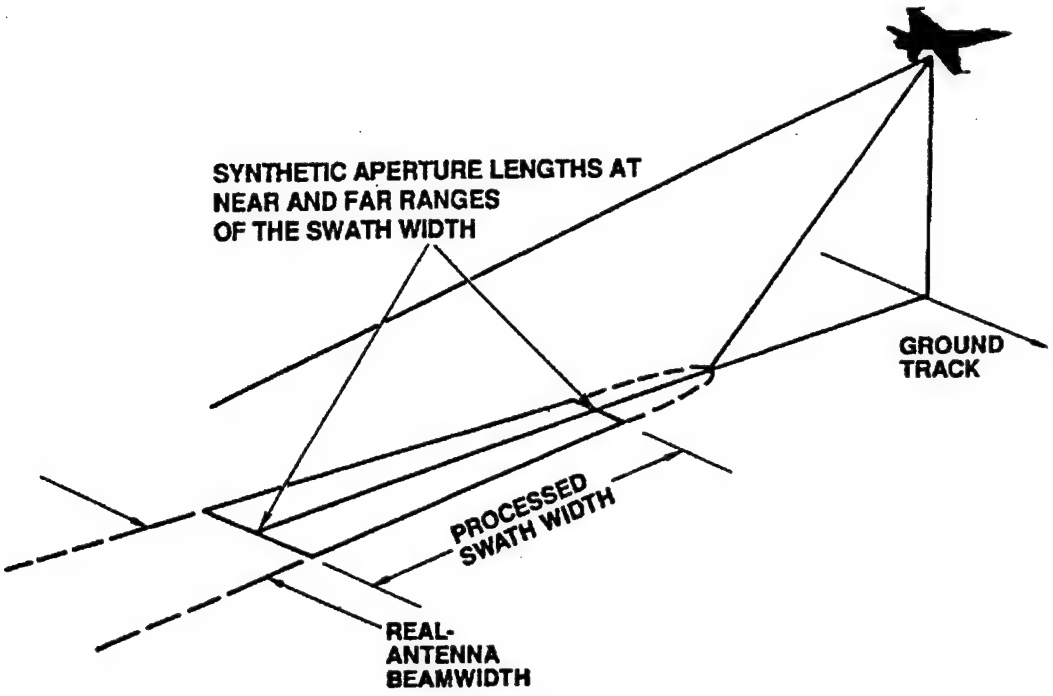

Figure 1. Side-Looking SAR [7]

Echo energy collected from each range resolved scatterer in the area to be mapped is made to arrive in phase at the output of the radar processor in order to realize the narrow beamwidth associated with the long, synthetically generated aperture. This is achieved by first correcting for all movement of the aircraft that deviates from straight line motion. At this point, we have what is known as an *unfocused* SAR. Then, for *focused SAR,* the *quadratic phase error is* corrected. Quadratic phase error is produced by straight-line motion of the radar past each point of the mapped area. Although most SAR systems are focused to improve the image quality, it is not necessary to add the increased mathematical complexity associated with it to the analysis presented in the following sections. The performance comparisons made for the nonuniform pulse repetition interval are independent of whether the SAR is focused or unfocused. However, a discussion of unfocused versus focused SAR will be presented in this section.

A second form of SAR is usually referred to as *spotlight* SAR. This is illustrated in Figure 2 in which the radar tracks a particular area of interest over some azimuth angle $\Delta\phi$. In this configuration the cross-range resolution is limited not by antenna size, as for side-looking SAR, but by target dwell time. Synthetic aperture length for small $\Delta\phi$ can be thought of as the tangential distance that the radar travels while moving through the angle $\Delta\phi$ to the target.

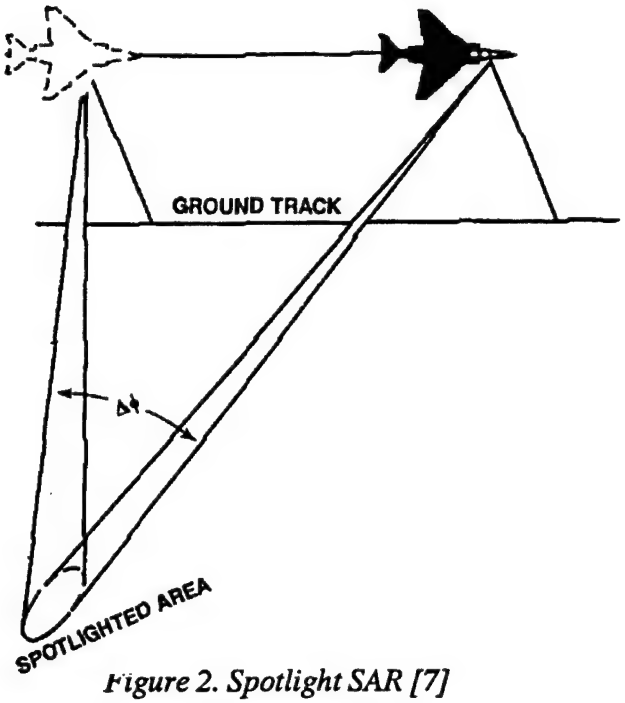

Figure 2. Spotlight SAR [7]

The third type of SAR is achieved by integrating echo energy as the antenna is scanned in azimuth. This is what is referred to as DBS, and is illustrated in Figure 3. In this case, for constant azimuthal scanning rate, a relatively long integration time will occur at portions of the scanning angle near the direction of platform motion, as compared with near broadside portions of the scan. Constant cross path resolution is normally a product of this configuration and effectively sharpens the real antenna beam. Side-looking SAR will be of primary interest during this research and will be discussed more thoroughly in the following sections.

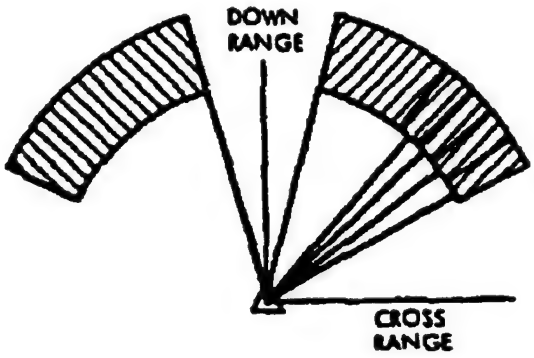

Figure 3. DBS [8]

B. Real Beam Radar Considerations

1. X-Direction Resolution

Pulse radars measure range by transmitting a pulse and timing the returned pulse from the target as shown in Figure 4 [6].

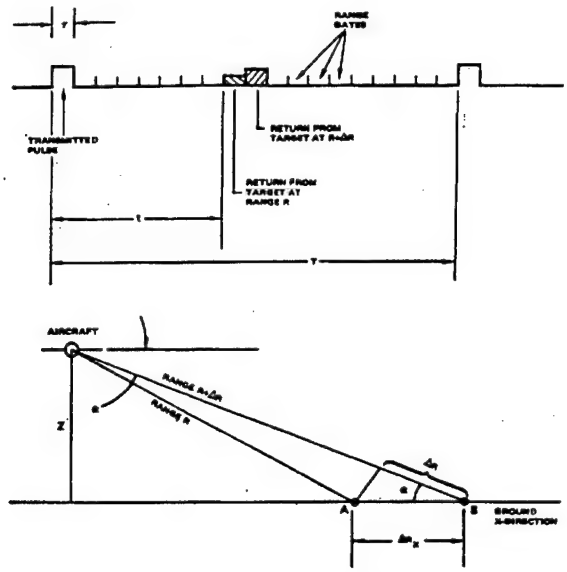

Figure 4. Resolution in the X-Direction [6]

This figure illustrates a transmitted pulse of duration τ with a PRI of T. The geometry of the radar platform and the ground can also be seen in Figure 4. If it is assumed that the range gates are of duration τ, two adjacent points on the ground, A and B, which are ΔRx apart, can be resolved if their returns occur in two separate range gates, as is shown in Figure 4. Because electromagnetic energy travels at the speed of light, c, it can be written that

$$t = \frac{2R}{c}; \; t + \tau = \frac{2(R + \Delta R)}{c} \tag{1}$$

where the factor of 2 in the equations above takes into account the round trip travel of the electromagnetic energy to the target. If one subtracts the two above equations, one gets

$$\tau = \frac{2\Delta R}{c}. \tag{2}$$

Also, from Figure 4 one can see that

$$\Delta R_x = \frac{\Delta R}{\cos\alpha}, \tag{3}$$

and finally, if one makes the appropriate substitutions then

$$\Delta R_x = \frac{c\tau}{2\cos\alpha} \tag{4}$$

where ΔRx is the resolution in the x-direction, which is perpendicular to the velocity vector. From Equation (4) the resolution in the x-direction is seen to be directly proportional to the pulsewidth τ; in other words, a short pulsewidth produces better resolution.

In a radar where the receiver is matched to the transmitted waveform, usually, the product of pulse duration τ and the receiver bandwidth W is unity

$$\tau W = 1; W = \frac{1}{\tau}. \tag{5}$$

Using Equation (5) in Equation (4), one obtains

$$\Delta R_x = \frac{c}{2W\cos\alpha}. \tag{6}$$

In the configuration shown in Figure 4, the maximum measurable range, R_{max}, is a function of the PRI, T, and given by

$$R_{max} = \frac{cT}{2}. \tag{7}$$

Beyond this range, the elapsed time between transmitted pulse and target return pulse will include multiples of the interpulse period, T, which results in ambigously measured range.

2. Y-Direction Resolution

As will be shown, the resolution in the y-direction of a real beam radar is proportional to the antenna beamwidth. For a circular antenna with a uniform current distribution, the radiation field intensity will involve first-order Bessel functions. The half power beamwidth in this case will be

$$\gamma = \frac{58.5\lambda}{D} \text{ (degrees)} \tag{8}$$

or

$$\gamma \cong \frac{\lambda}{D} \text{ (radians)} \tag{9}$$

where λ is the wavelength and D is the diameter of the antenna. In the following discussions, the value of γ will be approximated by Equation (9) where γ is given in radians.

It now becomes a matter of determining the resolution in the y-direction. From Figure 5 it can be seen that the resolution in the y-direction is

$$\Delta R_y = R\gamma \tag{10}$$

where R is the range to the resolution cell and γ is the antenna azimuth beamwidth. If the antenna is rectangular rather than circular, the beamwidth used in Equation (10) is determined by the equation

$$\gamma = \frac{\lambda}{l_1} \tag{11}$$

where l_1 is the cross-range dimension of the antenna.

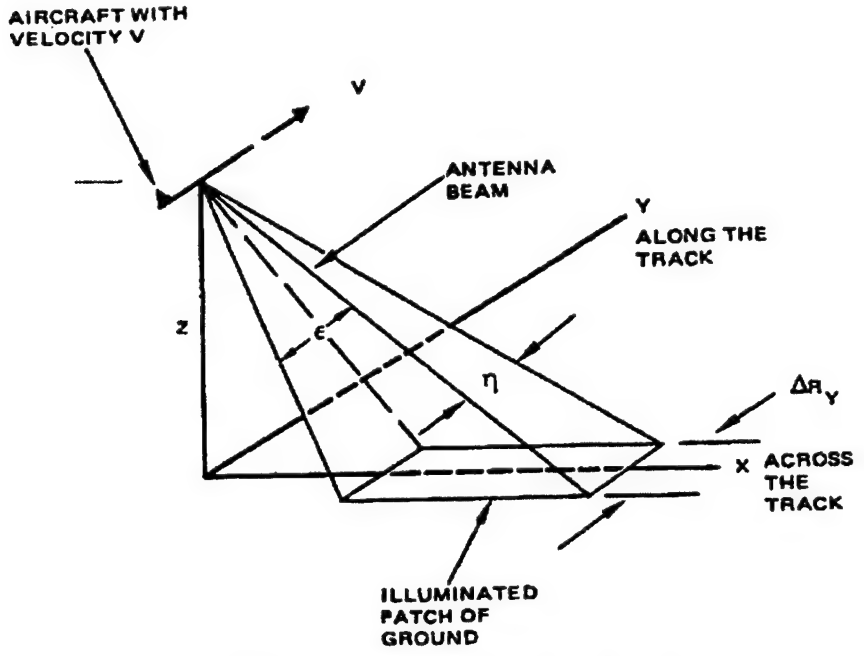

Figure 5. Geometry of a Real Array Imaging Radar [6]

C. SAR Basics

Synthetic array radars were invented to obtain images without using large antennas. In these radars the resolution in the x-direction is determined by the pulse duration as it was in the case of the real beam radar. However, the resolution in the y-direction is determined by using the Doppler information or spectral analysis as opposed to the beamwidth, which is the case for real beam radars. Thus, in SARs the effect is to simulate the return from a large array, i.e. narrow beam, by coherently integrating the returns from successive pulses from a small antenna as the radar platform moves. The result is to significantly increase the spectral signal processing which is required to produce equivalent resolution.

1. Phase and Frequency Relationships

If the transmitted waveform is as shown in Equation (12)

$$V_t = \sin 2\pi f_o t, \tag{12}$$

it can be represented as the waveform shown in Figure 6.

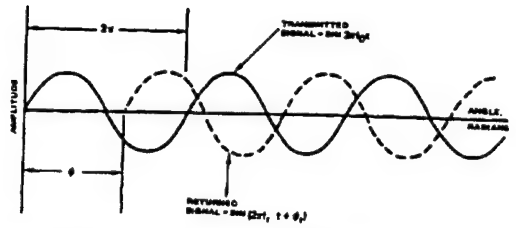

Figure 6. Transmitted and Received Signals from a Target [6]

If this signal is reflected from a moving target at a range R given by the equation

$$R = R_o + R't, \tag{13}$$

where R_o is the initial range, R' is the target's closing/opening rate in the direction of R, and t is the time; then returned signal at time t will be the signal which was transmitted Δt seconds ago with

$$\Delta t = \frac{2R}{c}. \tag{14}$$

If $t = t - \Delta t$ is substituted into Equation (12), the received signal is

$$V_r = \sin\left[2\pi f_o\left(t - \frac{2R_o + 2R't}{c}\right)\right]. \tag{15}$$

If the terms involving t are grouped together, then

$$V_r = \sin\left[t\left(2\pi f_o - \frac{2R'(2\pi f_o)}{c}\right) - \frac{2(2\pi f_o)R_o}{c}\right]. \tag{16}$$

Observation of Equation (16) shows that the coefficient of time, t, represents a frequency while the part not involving time represents a phase, ϕ. With this observation the returned signal V_r of Equation (16) will have a frequency of

$$2\pi f_r = 2\pi f_o - \frac{2R'(2\pi f_o)}{c} \tag{17}$$

and a phase

$$\phi_r = -\frac{2(2\pi f_o)R_o}{c}. \tag{18}$$

The value for the difference in transmitted and received frequencies, $f_r - f_o$, can be obtained by using the value of the transmitted frequency $2\pi f_o$ from Equations (12) and (17) as follows:

$$f_d = f_r - f_o = -\frac{2R'(f_o)}{c} = -\frac{2R'}{c/f_o} = -\frac{2R'}{\lambda} \tag{19}$$

where f_d denotes the Doppler shift and c/f is the wavelength λ. Therefore, one can see that the frequency of the returned signal from a moving target will be shifted in frequency from the transmitted frequency by an amount directly proportional to radar target closing rate and inversely proportionally to wavelength.

The equation for the phase angle of the returned signal, ϕ_r, as shown in Equation (18), can be written as follows:

$$\phi_r = -(2\pi)\frac{2R_o}{c/f_o}. \tag{20}$$

The number of equivalent wavelengths to the round trip distance $2R_o$ is represented by this equation. The role of the multiplier 2π is to convert the number of wavelengths to angle in radians. Therefore, the phase change is equivalent to a distance. Similarly, the Doppler shift in Equation (19) for an incoming target can be thought of as the number of wavelengths per second that the transmitted signal frequency is reduced by due to the closing rate R´. By definition frequency is the number of wavelengths per second.

In summary, the difference between transmit/receive frequencies is proportional to rate of change of the radar target range while the difference in phase of transmit/receive signals is proportional to radar target range. Thus, the phase is associated with range while the derivative of phase with respect to time (frequency) is associated with range rate.

2. Filter Principles

In radar systems the previously discussed frequency shifts are apparent in the spectral analysis of the returned signals from the target. These analysis can be carried out by either analog or digital methods. However, both methods basically convert a signal which is a function of time to a signal which is represented as a function of frequency.

Figure 7 shows the frequency equivalent of a time signal consisting of a sine wave of duration T [6]. Note the sin x/x behavior of the frequency function and the fact that the null to null frequency spread is 2/T. The 3 dB or half power bandwidth occurs at approximately 1/T with the first side-lobe to main lobe power ratio of -13.2 dB. Much in the same way as for antennas, various weighting functions can alter the characteristics of the main lobe and side-lobe filters as the requirements arise.

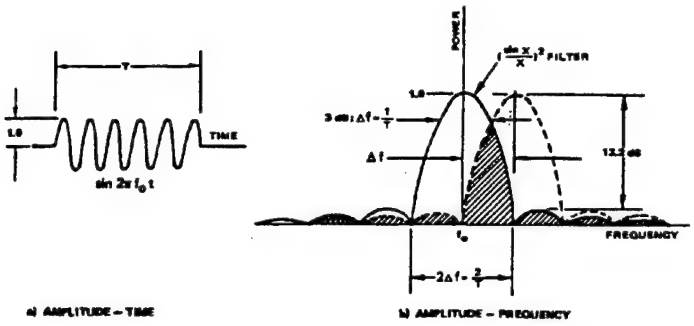

Figure 7. Frequency Spectrum of a Limited Duration Sinewave [6]

The frequency response of a filter to a function shifted in frequency by bandwidth Δf, i.e., the time function sin $2\pi(f_o+\Delta f)t$, is shown by the dashed curve of Figure 7B. The amplitude-frequency response is the same as that of sin $2\pi f_o t$ except for the fact that it is shifted by Δf. The filter response to the input sine wave of frequency, $f_o + \Delta f$, is represented by the dashed area of the figure where the two curves overlap. Therefore, the highest amplitude present will be 3 dB lower in power than that of a sine wave centered a frequency f_o. In addition, energy will be present in the filter side-lobes as shown.

a. Y-Direction Resolution

If one considers Figure 8, the process for determining the theoretical resolution in the y-direction can be illustrated. The radar platform is flying at velocity, V, parallel to the y-axis. The frequency difference between two ground points A and B which are D/2 apart, can be determined as follows.

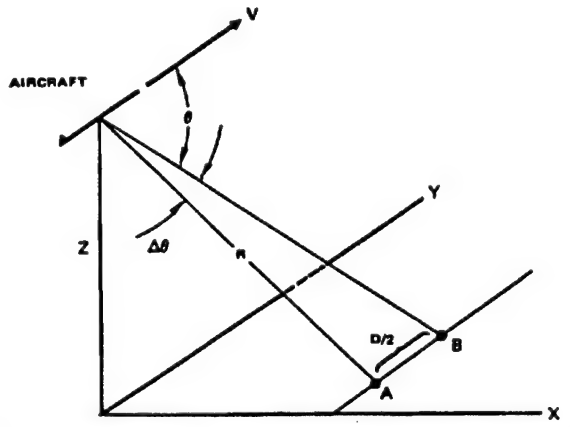

Figure 8. Resolution Element D/2 in the Y-Direction [6]

From the previous equations

$$f_B = \text{dopplershiftofpointB} = \frac{2V\cos\Theta}{\lambda} \qquad (21)$$

and

$$f_A = \text{dopplershiftofpointA} = \frac{2V\cos(\Theta + \Delta\Theta)}{\lambda}. \tag{22}$$

If the cosine term of Equation (21) is expanded in terms of sines and cosines and small angle relationships are used, i.e., $\cos\Delta\Theta \cong 1$ and $\sin\Delta\Theta \cong \Delta\Theta$, then the result is

$$\Delta f_i = f_B - f_A = \frac{2V}{\lambda}\Delta\Theta\sin\Theta. \tag{23}$$

The value of $\Delta\Theta$ from Figure 8 can be approximated by

$$\Delta\Theta \cong \frac{D}{2R} \tag{24}$$

where R is the range. If this is substituted into Equation (23), the result is

$$\Delta f_i = \frac{VD}{\lambda R}\sin\Theta. \tag{25}$$

The resolution in the y-direction $AR_y = D/2$ becomes

$$\Delta R_y = \frac{D}{2} = \frac{\lambda R\Delta f_i}{2V\sin\Theta}. \tag{26}$$

The y-direction resolution attained in Equation (25) is independent of beamwidth, as was not the case in a real beam radar. It depends primarily on the attainable frequency resolution, Δf_i, of the signal processing equipment.

In a radar system where the receiver is matched to the transmitted waveform, the duration of target illumination T should be $1/\Delta f_i$ [6]. In other words, during the data acquisition time T the radar platform flies a length of L = VT where V is the velocity. Thus, the equivalent antenna array length becomes

$$L = VT = \frac{V}{\Delta f_i} = \frac{\lambda R}{D\sin\Theta}. \tag{27}$$

If the numerator and denominator of Equation (26) are multiplied by T and the value of L from Equation (27) is used, the y-direction resolution is then

$$\Delta R_y = \frac{D}{2} = \frac{\lambda R}{2L\sin\Theta}. \tag{28}$$

The value of D/2 given by the above equation represents the best attainable y-direction resolution and is used in calculations as a figure of merit. However, in actuality the y-direction is obtained by a set of tuned filters.

b. Maximum Resolution

The maximum attainable y-direction resolution is determined by using the fact that the antenna illumination coverage on the ground should be greater than the equivalent antenna array length which was obtained in Equation (27). This is required to insure that the return of target energy from a point on the ground during the filter charge up time $T=1/\Delta f_i$. The results of Equation (27) yield

$$\frac{RL}{l} > L = \frac{\lambda R}{D \sin\Theta} \tag{29}$$

where l is the actual antenna length and L is the equivalent array length on the ground. Since $\Delta R_y = D/2$ for a sidelooking SAR, i.e., $\Theta = 90$ degrees, then

$$\Delta R_y \geq \frac{l}{2}. \tag{30}$$

Thus, the best resolution obtainable in the y-direction is one half of the actual antenna length, l.

c. Focused and Unfocused Arrays

From Figure 9 it can be seen that as the radar platform flies a distance L, a point on the ground appears at a distance R_1, R_o, and again at R_1.

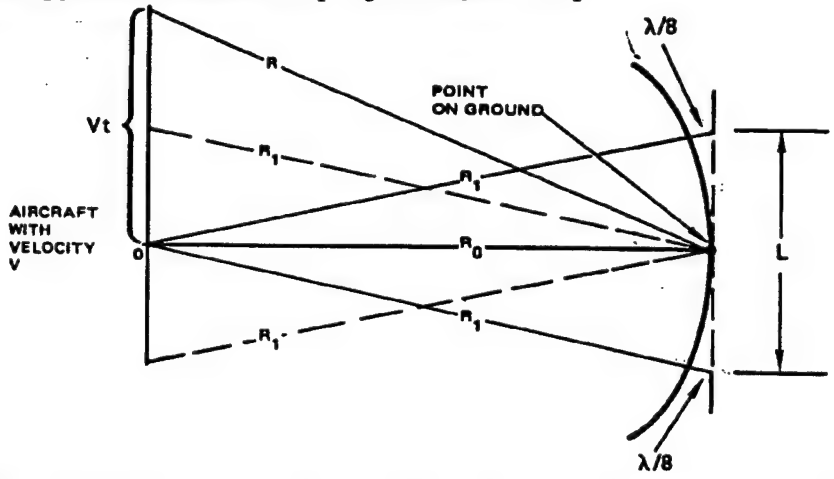

Figure 9. Range to a Point on the Ground as the Platform Flies with Velocity, V [6]

Because the phase of the arriving signal is proportional to the distance traveled, the phase of the returned signal will change with time. If a phase shift of 90 degrees, i.e. $\lambda/4$, is acceptable, before image degradation occurs and focusing is required, for a flight distance between zero to L, then based on the geometry and the Pythagorean Theorem the following equation can be written

$$(R_o)^2 + \left(\frac{L}{2}\right)^2 = (R_o + \lambda/8)^2 \tag{31}$$

$$R_o^2 + \frac{L^2}{4} = R_o^2 + \frac{\lambda R_o}{4} + \frac{\lambda^2}{64} \tag{32}$$

where $\lambda/8$ is the acceptable one-way phase change. If one neglects the last term and solves for L, then

$$L = \sqrt{\lambda R_o}. \tag{33}$$

If Equation (33) is substituted into Equation (28) and since a side-looking SAR scenario is assumed, i.e. $\sin\Theta = 1$, the y-direction resolution for an unfocused array is

$$\Delta R_y = \frac{D}{2} = \sqrt{\frac{\lambda R_o}{2}} \tag{34}$$

which is dependent on the square root of range R_o, in addition to the wavelength.

From the previous discussion it was shown that the phase angle of the return signal from a given point on the ground changes during a given observation time. It will be shown that the phase angle of the returned signal can be predicted. Hence, the return signal can be phase corrected and a longer length of data from the ground point can be used for signal processing. In a SAR system this phase correction is known as focusing, and SARs using this are called focused SARs.

Again, consider Figure 9 where the aircraft is at a distance Vt from zero and an aircraft to point on the ground range of R. The range R can now be written in terms of R_o and Vt as follows

$$R = [R_o^2 + (Vt)^2]^{1/2}. \tag{35}$$

If Equation (35) is expanded into a series, then

$$R = R_o + \frac{1}{2R_o}(Vt)^2 - \frac{1}{8R_o^3}(Vt)^4 + \dots . \tag{36}$$

Neglecting all terms following the second term of the equation we get

$$R - R_o = \frac{1}{2}\frac{V^2t^2}{R_o}. \tag{37}$$

Using Equation (37) and remembering that each wavelength is equivalent to a 2π phase shift. The equation for the phase shift can be written as

$$\phi = \frac{1}{2}(2\pi)\frac{V^2t^2}{\lambda R_o} = \frac{\pi V^2 t^2}{\lambda R_o}. \tag{38}$$

One important note is that Equation (38) is the one-way phase change; therefore, the two-way phase change will be twice this value.

d. Electronic Signal Processing

The function of the signal processor in a SAR is to store the incoming coherent returns for each range resolution element across the image width, and at the same time preserve the amplitude and phase of the returns across the Doppler frequencies of interest. After a synthetic array of length of data has been stored, the processor must perform the filtering process that has been discussed previously.

The two-way quadratic phase diagram for Equation (38) mentioned in the previous section is shown in Figure 10.

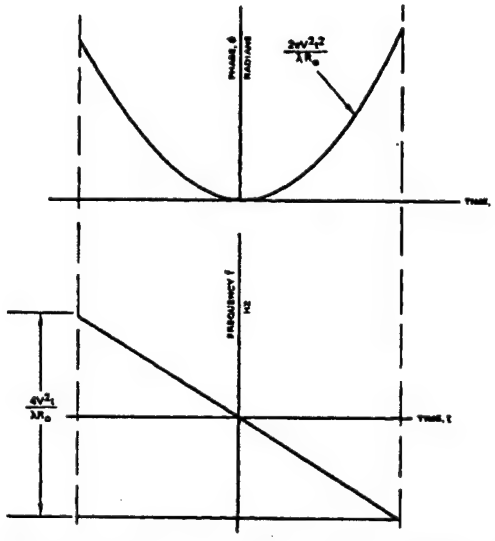

Figure 10. Phase and Frequency Excursion of a Single Point on the Ground as a Function of Time [6]

The quadratic phase equation, as written for two-way transmission and reception, is

$$\phi = \frac{2\pi V^2 t^2}{\lambda R_o}. \tag{39}$$

Angular frequency, ω, is defined as the rate of change of phase with respect to time $d\phi/dt$. Using this and Equation (39), we obtain

$$\omega = 2\pi f = \frac{d\phi}{dt} = \frac{4\pi V^2 t}{\lambda R_o}. \tag{40}$$

The two-sided frequency excursion will be twice this value as shown in Figure 10.

Keeping Figure 10 in mind, consider Figure 11. The radar platform is flying at a velocity, V, and has a beamwidth which can illuminate six points on the ground. In position A, the radar begins to illuminate point 1 and at position B it completes the illumination of this point [6]. At position A the component of the aircraft velocity vector along the vector A-1 will give rise to the frequency shift in the frequency-time diagram. As the platform flies from A to B this frequency will decrease, passing through zero as is shown in the bottom figure. Other points of the figure will also have the same frequency history with the total frequency excursion equal to $4V^2t/\lambda R_o$.

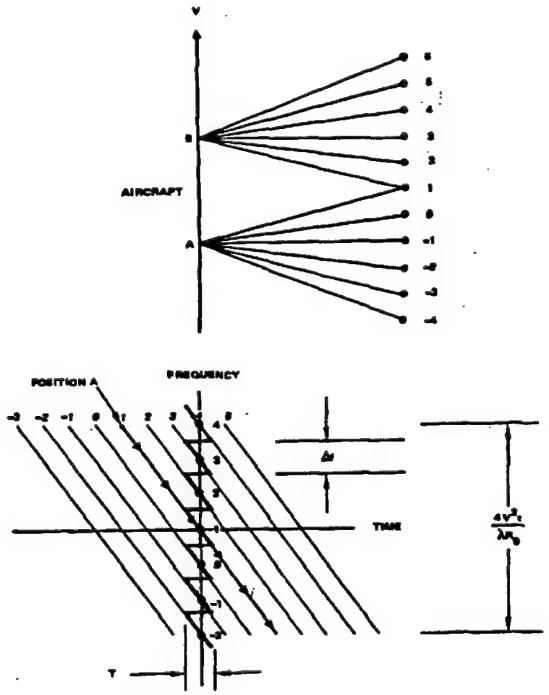

Figure 11. Platform Flight and Frequency History of Points on the Ground [6]

If focusing of the returned signal is not used, only the portion of the slanted frequency excursion of Figure 11 bounded by T can be used due to the overlapping frequency lines. Only the portion of data bounded by T of each data point -3, -2, -1, . . . can be used as input data. Using t = T/2 in the two-sided frequency excursion equation, we obtain

$$\Delta f = \frac{4V^2 t}{\lambda R_o} \tag{41}$$

which results in

$$\Delta f = \frac{2V^2T}{\lambda R_o}. \tag{42}$$

This frequency bandwidth corresponds to a time of T seconds ($\Delta f = 1/T$).

Reducing Δf, or equivalently increasing the y-direction resolution, will require focusing of the returned signal. Focusing will effectively allow the utilization of frequency excursions from various ground points without interference between frequency returns of these points. Based on the previous background it becomes a simple matter to see that the electronic signal processing of synthetic array radars can be accomplished by a set of range gates, for x-direction resolution, and a set of Doppler filter for each range gate for the resolution in the v-direction. This principle is shown in Figure 12.

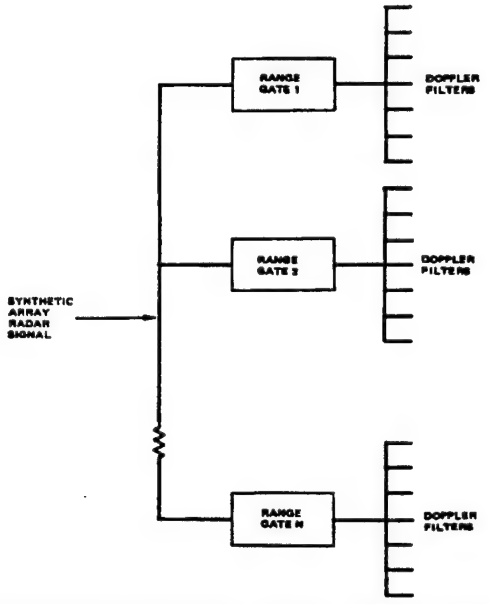

Figure 12. Range Gates Followed by Doppler Filters for Electronic Data Processing

Figure 13 shows the 3dB beamwidth coverage and associated maximum and minimum ranges to the ground in the vertical plane [6]. The range resolution element, d_r, is also shown. The number of range gates can be calculated as follows

$$N_R = \frac{R_{max} - R_{min}}{d_r} = \frac{R\lambda}{ld_r \tan\alpha} \tag{43}$$

where N_R is the number of range gates, $d_r = c\tau/2$ is the range resolution along R with τ being the pulse duration and c is the velocity of propagation. The second equation determines the value of N_R in terms of an average range, R, and the antenna beamwidth $\Theta_{BW} = \lambda/l$.

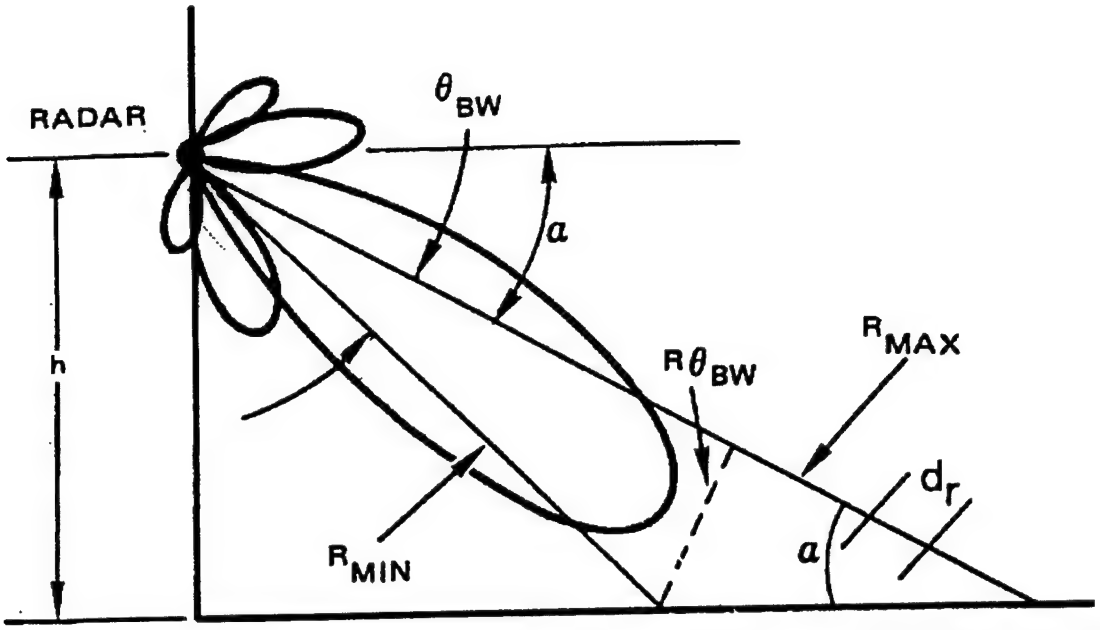

Figure 13. Maximum and Minimum Range-to-Ground for the 3dB Antenna Beamwidth, Θ_{BW} [6]

Since $d_r = \Delta R_x \cos\alpha$, Equation (43) becomes

$$N_R = \frac{R\lambda}{l\Delta R_x \sin\alpha}. \tag{44}$$

The highest frequency within the synthetic array length, or maximum frequency excursion can be obtained from Equation (42) by substituting VT = L to obtain

$$(\Delta f)_L = \frac{2VL}{\lambda R_o}. \tag{45}$$

Using the value of $L = \lambda R/D$ for the side-looking SAR case, i.e. $\Theta = 90$ degrees, and using Equation (27), we obtain

$$(\Delta f)_L = \frac{2V}{D}. \tag{46}$$

The Nyquist sampling theorem says that the number of time samples for representing a given frequency should be at least twice that frequency. Therefore, in this case the number of samples per second will be $2(\Delta f)_L$. Because these samples are taken within the time that it takes to fly a synthetic array length L, the total number of samples will be

$$N_D = 2(\Delta f)_L T = \frac{4V}{D} \cdot \frac{\lambda R}{VD} = \frac{4\lambda R}{D^2}. \tag{47}$$

The value of $T = 1/\Delta f_i$ is obtained by using Equation (25) with $\Theta = 90$ degrees.

The total number of samples, N, for all range gates N_R, i.e. Equation (42), is

$$N = N_R N_D = \frac{(R_{max} - R_{min})}{d_r} \frac{4\lambda R}{D^2}. \tag{48}$$

Using the value of N_R from Equation (44) and denoting the azimuth resolution D/2 by ΔAZ, we obtain another form of Equation (48) as

$$N = \frac{R\lambda}{l(\Delta R_x)\sin\alpha} \frac{R\lambda}{(\Delta AZ)^2}. \tag{49}$$

From Equation (49) it can be seen that the number of samples is directly proportional to the square of distance R and is inversely proportional to resolution in the range and cross-range directions. Equations (48) and (49) are used in determining the signal processing requirements of SARs.

Major parameters in the design of a synthetic aperture radar are the bounds of the Pulse Repetition Frequency (PRF) of the transmitted signal. The bounds placed on the PRF are determined by the mapping range of the radar and the Doppler frequency shift of the extreme points of the antenna coverage. The Doppler shift between points A and B can be determined from Figure 14 and is given by

$$f_d = \frac{2V}{\lambda}\cos\Theta - \frac{2V}{\lambda}\cos(\Theta - \Theta_{BW}) \tag{50}$$

where Θ_{BW} is the 3 dB antenna beamwidth.

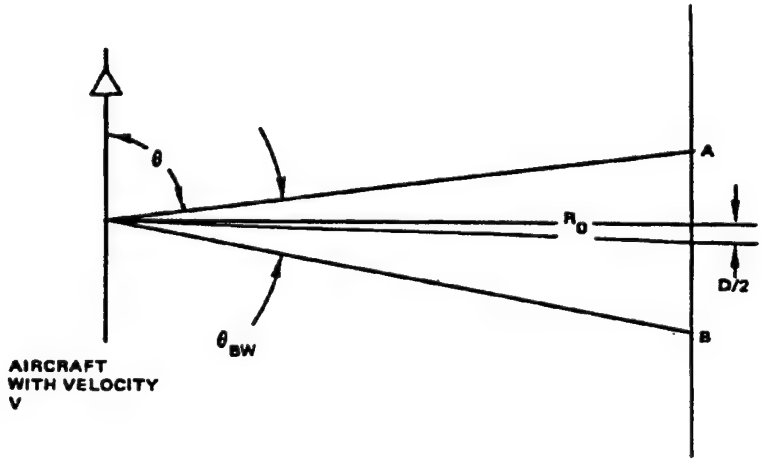

Figure 14. Ground Coverage in the Y-Direction for a 3 dB Beamwidth, Θ_{BW} [6]

If the small angle approximation for Θ_{BW} is used, the above equation reduces to

$$f_d = \frac{2V}{\lambda}\Theta_{BW}(\sin\Theta). \tag{51}$$

For a side-looking SAR, Θ = 90 degrees, and if the relationship $\Theta_{BW} = \lambda/l$ where λ is the wavelength and l is the antenna length is used, Equation (50) becomes

$$f_d = \frac{2V}{l}. \tag{52}$$

Figure 15 shows the frequency representation of a train of pulses with a PRI of T.

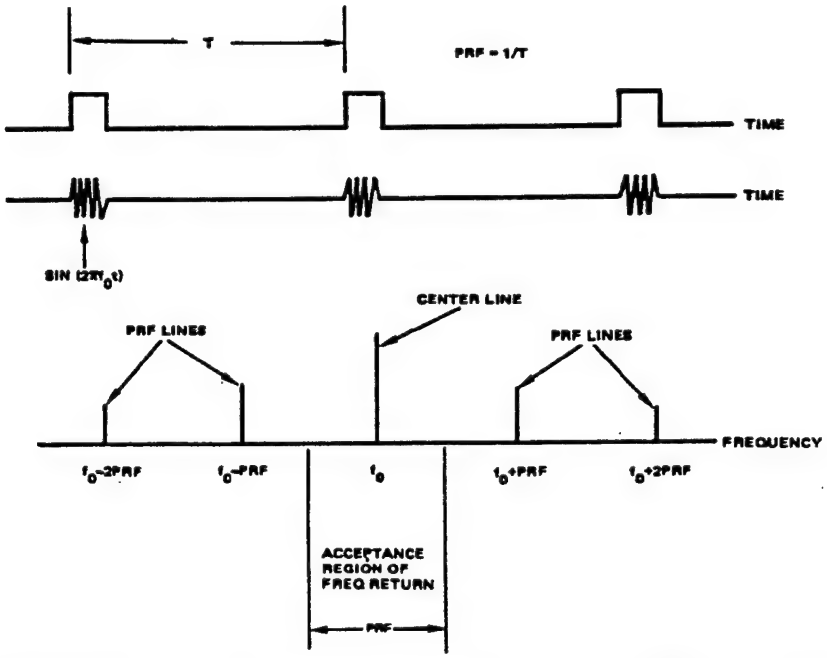

Figure 15. Transmitted Pulse and Spectral Diagram of PRF Lines [6]

If it is assumed that the Doppler shift excursion of Equation (41) should fit around the center frequency, f_o, then

$$f_d \leq \text{PRF}, \tag{53}$$

and

$$\text{PRF} \geq \frac{2V}{l}. \tag{54}$$

Equation (54) insures that the ground return from other PRF lines will not interfere with the return from the transmitted frequency f_o.

By using the maximum desirable mapping range and the fact that the returned pulse from this range must come within the interpulse period T, we can obtain the upper limit. If this condition is met, it will help insure that there will not be a problem with range ambiguities. Therefore, this upper limit can be written as

$$T \geq \frac{2R_{max}}{c} \tag{55}$$

where R_{max} is the maximum mapping range. Using the relationship T = 1/PRF, then we can write the equation for the upper limit as

$$PRF \geq \frac{c}{2R_{max}}. \tag{56}$$

If Equations (54) and (55) are combined, the limits for the PRF can be obtained from

$$\frac{2V}{l} \leq PRF \leq \frac{c}{2R_{max}} \tag{57}$$

where the lower limit is defined by the platform velocity and antenna and the upper limit is defined by the maximum mapping range.

IV. THEORY RELATED TO NONUNIFORM PRI

A. Definition of Nonuniform PRI

In a SAR the transmitted waveform consists of a train of pulses which are coherently integrated in order to obtain the desired cross-range resolution for the image. To perform the analysis that will be presented in the following section, there were several basic assumptions that were made. It was assumed that all the pulses were rectangular, that they were modulated with the same carrier frequency, and that they were of the same duration.

A SAR, as with any radar system in general, samples each pulse of the Doppler shifted return signal. The spacing between the pulses is referred to as the pulse repetition interval or PRI. When the spacing between the transmission of the pulses is varying with time, the PRI is said to be nonuniform. As shown in References 3 and 9, the received sample sequence for one range bin of a uniform train of pulses is mathematically defined as

$$s_k = C_R e^{j2\pi f_d T k}, \tag{58}$$

where s_k = The sample corresponding to the k^{th} pulse
C_R = Complex voltage determined from system parameters and range bin
f_d = Doppler Frequency
T = PRI.

The product, Tk in Equation (58) represents the time at which the k^{th} pulse is sampled. Therefore, in a similar manner the sequence for a nonuniform PRI can be defined as

$$s_k = C_R e^{j2\pi f_d T_k} \tag{59}$$

where T_k = time to k^{th} inter-pulse interval.

B. Waveform Processing Concepts

As was mentioned earlier the concern with a SAR waveform, in general, is the presence of side-lobes in the adjacent Doppler filter. These side-lobes can potentially produce a smearing effect in the azimuth dimension of the image. Thus, a nonuniform PRI waveform design must either inherently control the side-lobes or be accompanied by signal processing techniques which will provide sufficient side-lobe suppression so that the image quality is not significantly degraded.

The results in Reference 10 show that the effect of staggering the PRI of a pulse train is to smear the pronounced Doppler ambiguities, with this effect increasing with disance from the main beam. The structure of the main beam remains essentially unchanged because it is not possible to design a nonuniform PRI waveform so that the side-lobes between the ambiguities are suppressed as far as those for a uniform waveform at the nominal PRI [10], the side-lobe suppression must be performed in the signal processing portion of the system.

One method for implementing a nonuniform PRI and at the same time possibly be able to sufficiently suppress the side-lobes is described in References 1 and 2. This technique will be used in Section V to examine the feasibility of creating an image with a SAR using a nonuniform PRI. However, the major principles of this technique will be summarized below before the results are presented.

C. Interpolation Method for Processing Nonuniform Pulse Trains

One method which has been successfully used to improve the performance of a non-uniformly sampled sequences is described in References 1 and 2. This method is based on a linear interpolator, operating on a block of M nonuniformly spaced samples, which is used to interpolate M-2 equally spaced sample values. Because both the interpolator and the filter are linear, their composition is linear and the result is the desired set of weights [1].

The weight calculation is mechanized by first forming the minimum energy interpolation of M unequally spaced sample points. The minimum energy band limited interpolator, $x_{ME}(nT)$, for the n^{th} interpolated point on a spacing of T is given by

$$\hat{x}_{ME}(nT) = \sum_{p=1}^{M} s_p \sum_{q=1}^{M} a_{qp} \frac{\sin 2\pi W(nT - t_q)}{2\pi W(nT + -t_q)} \tag{60}$$

where s_p = p^{th} value of a nonuniformly sampled sequence,
W = selectable parameter controlling the bandwidth over which the interpolator assumes signals are present,
a_{qp}= the qp element of A^{-1} where A is an M x M matrix given by

$$A = \begin{bmatrix} \frac{\sin 2\pi W(t_1 - t_1)}{2\pi W(t_1 - t_1)} & \cdots & \frac{\sin 2\pi W(t_M - t_1)}{2\pi W(t_M - t_1)} \\ \cdot & \cdot & \cdot \\ \frac{\sin 2\pi W(t_1 - t_M)}{2\pi W(t_1 - t_M)} & \cdots & \frac{\sin 2\pi W(t_M - t_M)}{2\pi W(t_M - t_M)} \end{bmatrix}. \tag{61}$$

In Equation (62) t_M is the sample time for the M^{th} nonuniformly sampled pulse. Due to the fact that s_p is a function of frequency, the entire matrix $x_{ME}(nT)$ must be calculated for each frequency over the Doppler frequency range of interest. Therefore, x_{ME} is actually a function of both nT and Doppler frequency. Since each value of $x_{ME}(nT)$ in Equation (61) is a linear sum of sample values, the cascaded filter given by Equation (62) is also a linear sum of the original sample values. Thus,

$$S(f) = \sum_{n=1}^{M} w_n x_{ME}(nT) e^{-j2\pi f_d nT} \tag{62}$$

where f = frequency for which $x_{ME}(nT)$ was calculated,

w_n = the weighting function

f_d = the center frequency of Doppler filter.

The interpolation matrix, A, only requires knowledge of the sample times and the selected bandwidth but no other values. It can be entirely precomputed since it does not depend on the sample values. The interpolation matrix is valid only for a particular output sequence and must be recomputed if the sample sequence changes. This is significant in radar applications. The random PRIs can be predetermined and programed into the radar transmitter, thus the matrix can also be precomputed and stored in the signal processor to save processing time. If the random sequence changes from one coherent integration interval to the next, then more than one matrix would have to be precomputed and stored in the radar system.

The value of W is very important as it determines the frequency range over which the cascaded filter will be effective. As will be shown in the following section, the choice cannot be made arbitrarily.

V. ANALYSIS AND RESULTS OF INTERPOLATION BASED APPROACH

The main objective of this section will be to present the results of the analysis performed to examine the feasibility of using interpolation to reduce the side-lobes resulting from a nonuniform PRI. In order to accomplish this two different SAR scenarios were considered. The basic parameters of the two scenarios are defined in Table 1. The parameters of the two cases were chosen because of the variations in the requirements on the PRI, Scenario A requires a much higher PRF than Scenario B. Scenario A is a typical scenario for a missile platform imaging an area, where Scenario B might be typical of aircraft or helicopter reconnaissance situations. More details of the parameters which were used in Scenario A and Scenario B to perform the analysis are presented in Appendixes A and B, respectively.

The most important parameter which had to be determine for these cases were the PRI and the appropriate bounds for the particular scenario. The lower bound was chosen to avoid range ambiguities, and was determined based on Equation (63),

$$PRI_{min} = \frac{2*R_{max}}{C}. \tag{63}$$

Table 1. Basic Parameters of Scenarios Analyzed

	Scenario A	Scenario B
Frequency	35 GHz	10 Ghz
Range	2 km	10 km
Antenna Diameter	.125 m	.61 m
Velocity	100 m/sec	300 m/sec
PRF_{min}	40 kHz	6.1 kHz
PRF_{max}	71.4 kHz	9.2 kHz
PRF_{avg}	55 kHz	7.7 kHz

This requirement is a necessity for an imaging radar. The minimum PRI for Scenario A was determined to be 14 microseconds (μsec), which corresponds to a maximum PRF of 71.43 kHz, the corresponding minimum PRI for Scenario B was determined to be 108.7 μsec which corresponds to a maximum PRF of 9.2 kHz. The average performance of each scenario was evaluated based on the amount of energy present in the main beam compared to the side-lobes and also the peak response of the main beam compared to the peak of the first side-lobe.

The value chosen for the upper bound for the PRI was a little more subjective. With the inverse relationship between PRI and PRF, the maximum PRI can be chosen based on the minimum PRF. It was shown in Reference 2 that the band limit used in the interpolation process should be less than 50 percent of the average sample rate. Also, the way the interpolator works is that the band limit determines the values over which the frequency response is essentially equal to the uniform PRI case; therefore, the larger the band limit can be the better the performance, i.e. ISL, will be. Based on these factors, the minimum PRF for Scenario A was selected to be 40 kHz. The maximum PRI now becomes 25 μsec. For Scenario B the minimum PRF was determined to be 6.1 kHz, which corresponds to a maximum PRI of 164 μsec, this bound was chosen for comparison purposes, in order to provide the same percentage of randomness as Scenario A.

With the reasoning behind the selected bounds on the PRI established, the actual bounds for Scenarios A and B were then determined to be between 14.0 and 24.7 μsec and 108.7 and 164 μsec, respectively. These bounds produce average PRI's of approximately 17.9 and 130 μsec, or average PRFs of approximately 55 and 7.7 kHz; respectively. As was stated in Section I, the performance of the different waveforms will be quantified in terms of the integrated side-lobe level and the peak side-lobe level. These quantities will be calculated for each case considered, based upon the curve which is the product of the frequency response of the sampled sequence and the antenna pattern for a 6-inch circular aperture antenna for Scenario A and a 24-inch circular aperture for Scenario B. In order to perform the product of the frequency response and the antenna pattern one of them must be translated into the coordinates of the other based on the relationship

$$f_d = \frac{2V}{\lambda}\cos\theta, \tag{64}$$

which is the first-order definition for the Doppler frequency. The radiation pattern for the antenna that was used for Scenario A is shown in Figure 16, and the pattern for Scenario B is shown in Figure 17.

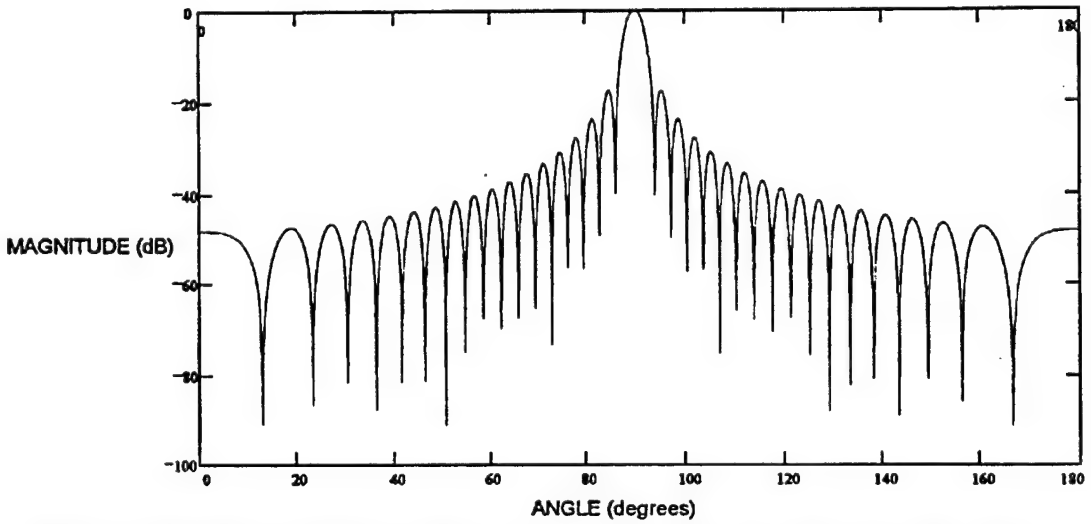

Figure 16. Antenna Radiation Pattern for a 6-Inch Circular Antenna at 35 GHz

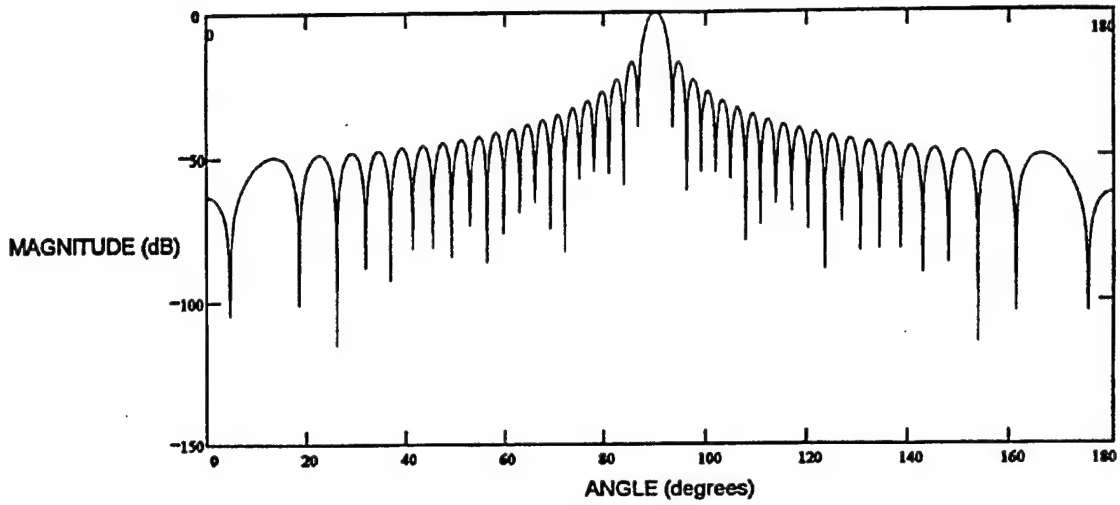

Figure 17. Antenna Radiation Pattern for a 24-Inch Circular Antenna at 10 GHz

In the following discussion there will be several different waveforms examined to establish the relative performance as it applies to the SAR scenarios which were described above. The different waveforms examined include a uniform PRI waveform at the average PRF, two non-uniform PRI waveforms and four interpolated nonuniform PRI waveforms. The nonuniform PRI cases included two different degrees of randomness; the narrow case had a random variation between ± 5 percent about the nominal PRF, whereas in the wide case the inter pulse spacing was random over the entire range that was determined to be feasible. These two cases, as well as the uniform case, served as a point of comparison of the performance improvement provide by the interpolation method. In the remainder of the cases the interpolation performance was illustrated. This consists of interpolating the randomly spaces samples of the above cases to equally spaced samples at the nominal pulse spacing. After interpolation, a four sample Blackman-Harris Window [11] was applied as the low pass filter. The frequency response was computed by performing a Discrete Fourier Transform of the weighted sampled sequence, i.e. Equation (62), for the doppler filter center at zero hertz. The band limit of the input signal required for the interpolator was selected to be two different values for performance comparison. The product of each these frequency responses and the appropriate antenna pattern of either Figure 16 or 17 was performed, followed by the calculation of the ISL and PSL. Where the ISL is the ratio of energy in the main beam to energy in the side-lobes and the PSL is the ratio of the peak of the main beam to the peak of the first side-lobe. Finally, one of the interpolated cases was selected and Monte Carloed over the random PRI distribution in order of confirm that the results obtained were representative of the average performance.

The initial emphasis of the analysis was placed on the system described by Scenario A. The first case to be examined was the uniform PRI case. This case served as a point of comparison. Each case to be examined was weighted by a four sample Blackman-Harris Window. For each case there were two figures which were of importance. The first was the weighted frequency response. The other curve of interest was the product of the frequency response and the antenna pattern. The weighted frequency response of the uniform case can be seen in Figure 18, followed by the product of the antenna pattern and the frequency response in Figure 19. The frequency response in Figure 18 appears as theoretically expected. The peak at zero has a value equal to 44 dB, i.e. 20*log(.36*Number of pulses) [2 and 10], where the number of pulses equals 479, and the first side-lobes are approximately 92 dB down from the main lobe. Both the .36 factor and the

-92 dB side-lobes are characteristics of the four-sample Blackman-Harris Window. Also, the Doppler ambiguities appear at multiples of the PRF as expected. The ISL and PSL for this case were determined to be 93.581 dB and 97.347 dB, respectively.

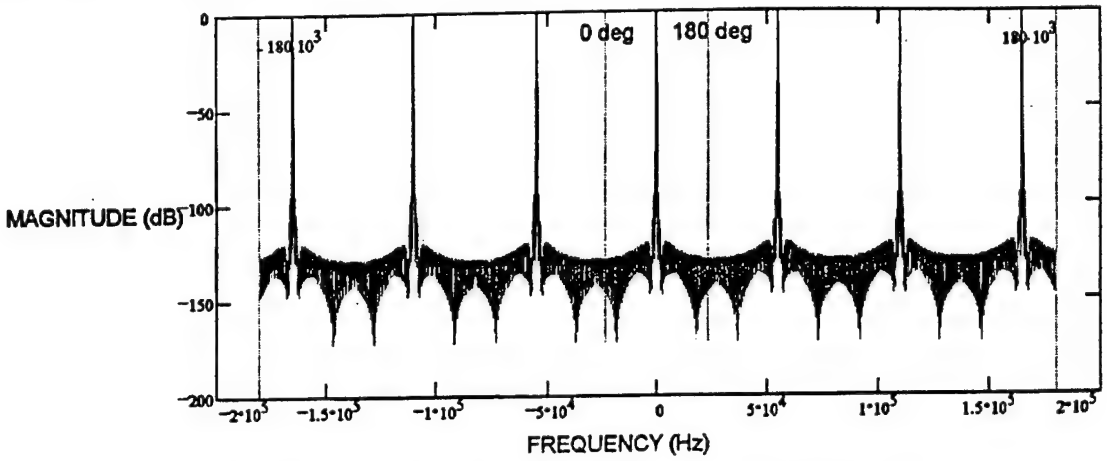

Figure 18. Frequency Response for a Uniform PRF of 55 kHz

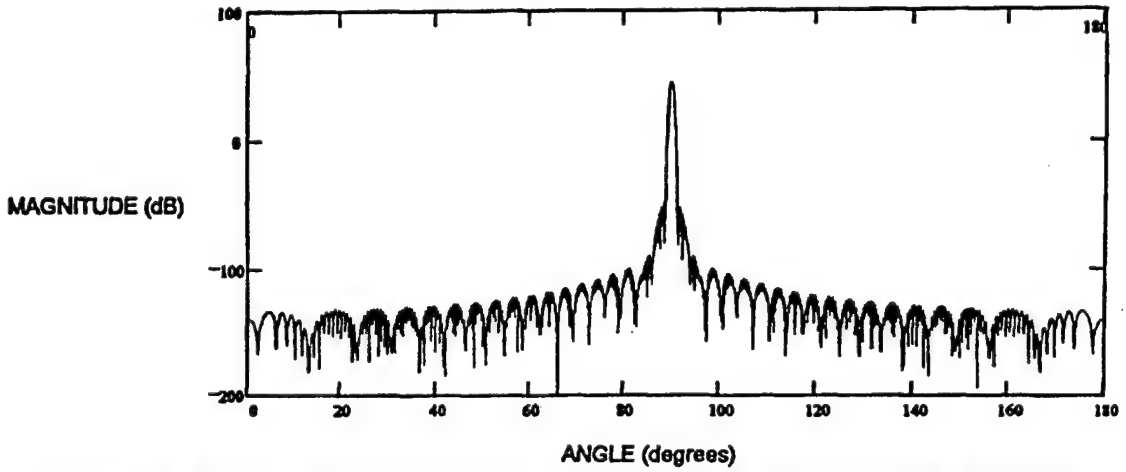

Figure 19. Product of Response and Antenna Pattern for Uniform PRF of 55 kHz

The following two cases examined were the nonuniform PRI cases. Figures 20 and 21 show the curves which correspond to the narrow case i.e. ±5 percent. As was expected, the main beam has a value of approximately 44 dB; however, the side-lobe structure is now different. The side-lobes around the main beam now appear at approximately 54 dB below the main beam, i.e. 20*log (Number of Pulses), [2 and 8]. From Figure 20, one can also see a decrease in the magnitude of the ambiguity responses as they get farther from the main beam. However, with the narrow variation there is still a substantial response at multiples of the input frequency. The nonuniform variation is insufficient to unambiguously determine the frequency of signals at multiples of the nominal sample rate. The ISR and PSR for this case were found to be 16.501 dB and 62.379 dB, respectively.

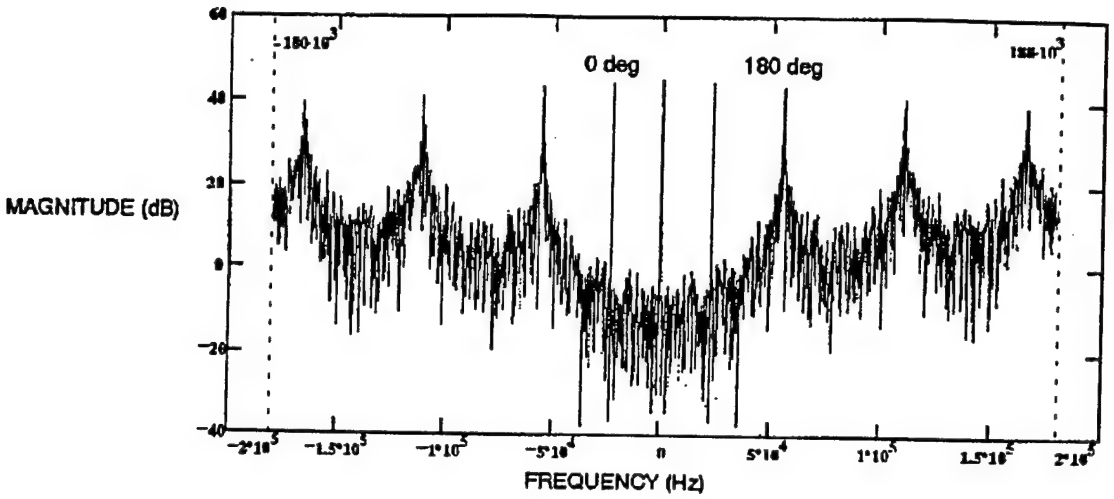

Figure 20. Frequency Response for ±5 Percent Random Variation of PRF About 55 kHz

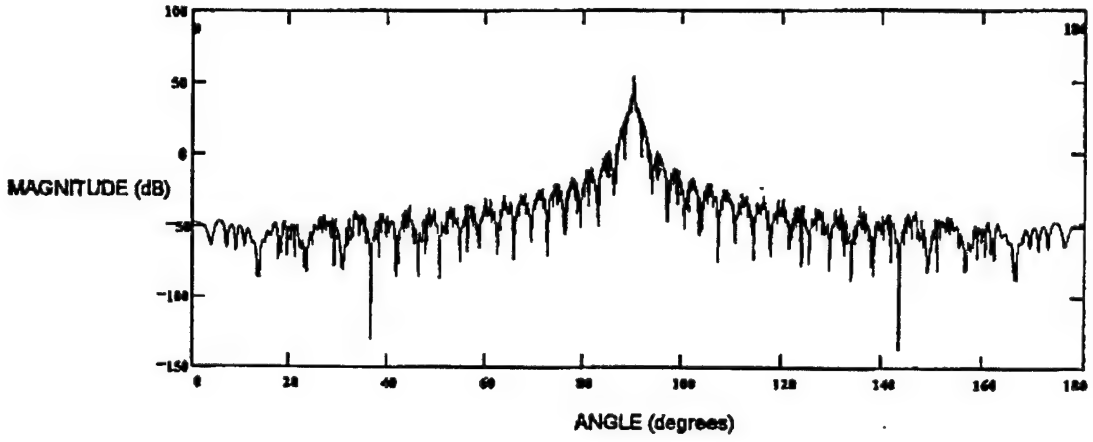

Figure 21. Product of Response and Antenna Pattern for ±5 Percent Random Variation About a PRF of 55 kHz

The corresponding plots for the case of wide variation are shown in Figures 22 and 23, and are shown to have an ISL of 9.918 dB and a PSL of 48.676 dB. The structure of Figure 22 is as expected with the main beam magnitude and side-lobes essentially unchanged. However, the ambiguous responses are substantially suppressed, although the side-lobes are raised. Note that the ambiguous response is still apparent at 55 kHz. A high degree of nonuniformity is required to totally suppress the ambiguous responses. The frequency response is poor compared to the uniform case with the same sample window.

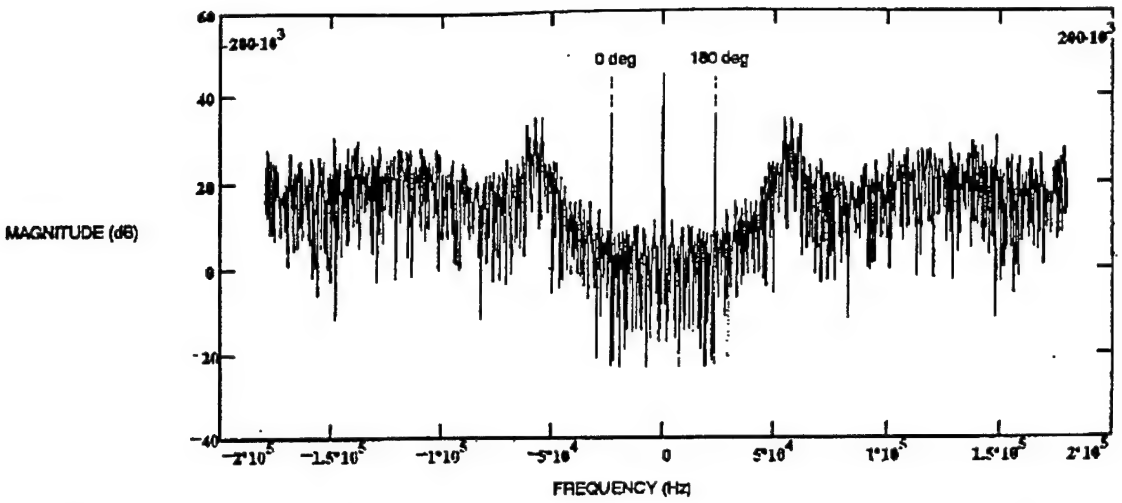

Figure 22. Frequency Response of Widely Random Variation of PRF About 55 kHz

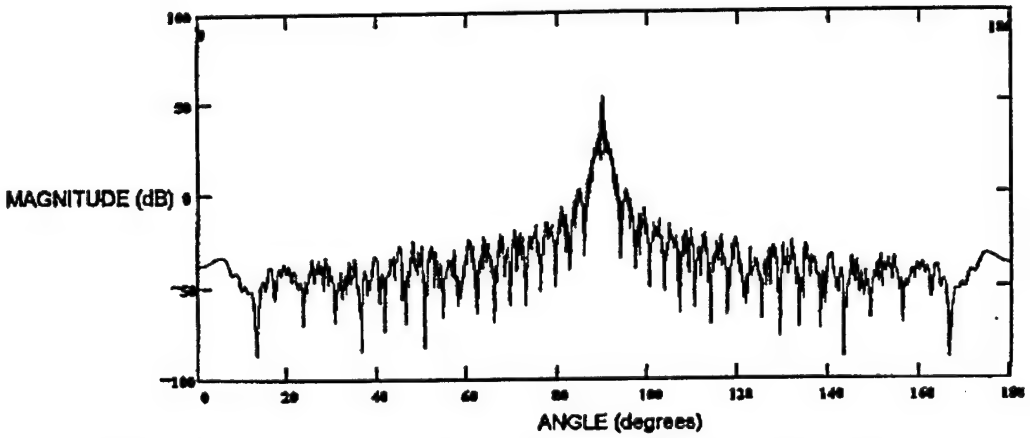

Figure 23. Product of Response and Antenna Pattern for Widely Random Variation of PRF About 55 kHz

The next set of configurations to be considered were the interpolated nonuniform sampled sequences. For each of the degrees of randomness the band limiting parameter was varied. Two values for this parameter were chosen to examine their effects. These values were selected to be 20 kHz and 30 kHz, for Scenario A based on the results presented in Reference 6. It was shown that performance degrades for values greater than 50 percent of the average sample rate (for I/Q sampling) [6].

In Figures 24 and 25 the effects of interpolation of a narrow random variation sequence are shown. The band limit was set to 20 kHz. Within the bounds of the band limit selected, the response is essentially equal to that of a uniformly sampled sequence. Outside these bounds the response behavior is similar to the uninterpolated case. The main beam had a magnitude of approximately 44 dB and the returns within the bounds of the band limiting parameter are about 92 dB below the main beam. For frequencies whose magnitude is greater than the value set for the band limit the side-lobes are at approximately -53 dB, which is the value determined for the side-lobes of the nonuniform uninterpolated case. The integrated side-lobe level and the peak side-lobe level were determined to be 69.213 dB and 96.954 db, respectively.

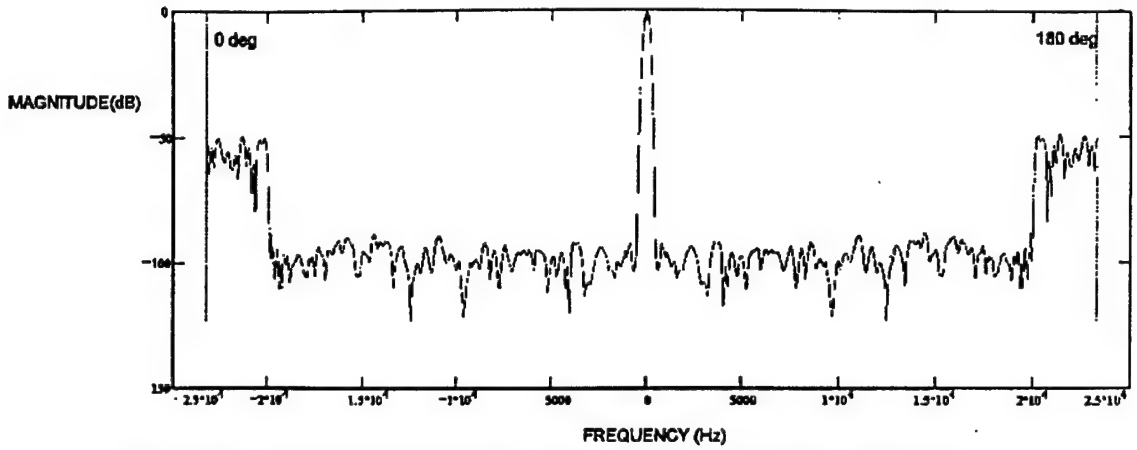

Figure 24. Frequency Response of Interpolation for the ±5 Percent Random Variation with W = 20 kHz

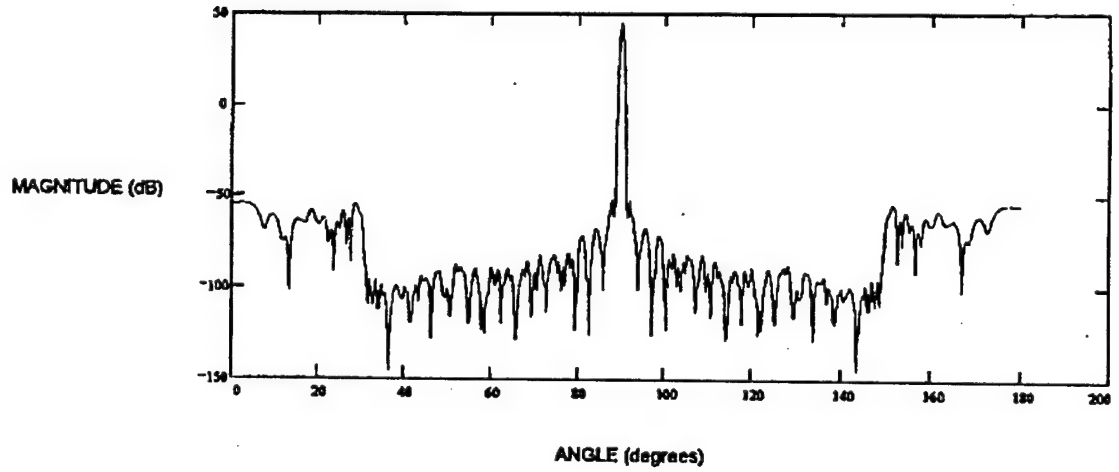

Figure 25. Product of Response and Antenna Pattern for Interpolation of ±5 Percent Random Variation with W = 20 kHz

Next, the band limit was selected to be 30 kHz. These effects are plotted in Figures 26 and 27. As expected the performance showed some degradation. The side-lobes within the bounds of the band limit are somewhat higher and the response is not as distinct within the band limit as it was for the case where the band limit was 20 kHz. Outside the band limit the response is essentially the same as the uninterpolated case. The ISL for this case was determined to be 68.663 dB and while the PSL was found to be 84.611 dB.

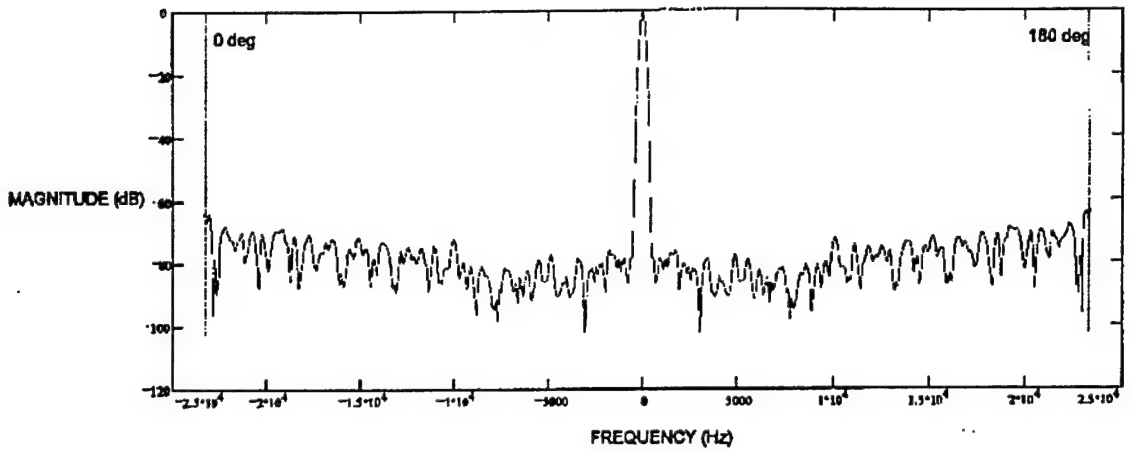

Figure 26. Frequency Response of Interpolation for ±5 Percent Random Variation About 55 kHz with W = 30 kHz

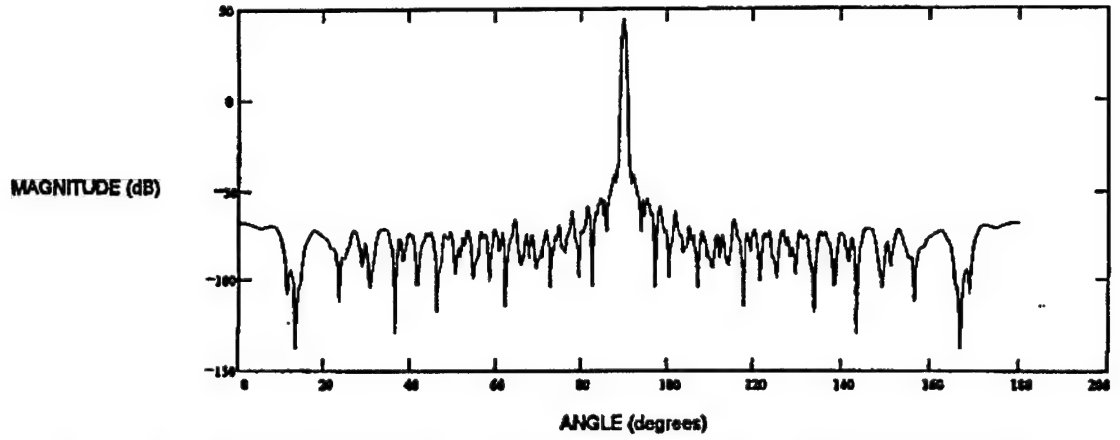

Figure 27. Product of Response and Antenna Pattern for ±5 Percent Random Variation Interpolation with W = 30 kHz

In the plots to follow the previous two sets of results were repeated for wide sample variation. Firstly, the band limit was set to 20 kHz. These results are plotted in Figures 28 and 29. The main beam still maintains a magnitude of about 44 dB, and the side-lobes within the band limit are at approximately 80 dB down from the main beam. Outside the boundary set by the 20 kHz band limit the response is essentially equal to the uninterpolated response. The ambiguous response is suppressed in comparison with the narrow variation but the side-lobes are raised. The ISL for this case was determined to be 54.724 dB and the PSL was determined to be 85.649 dB.

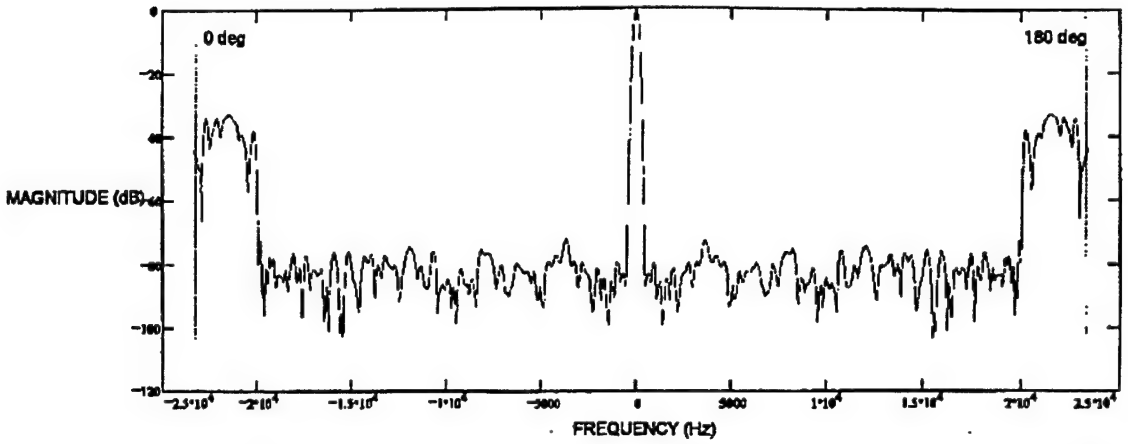

Figure 28. Frequency Response of Interpolation with Widely Random Variation and W = 20 kHz

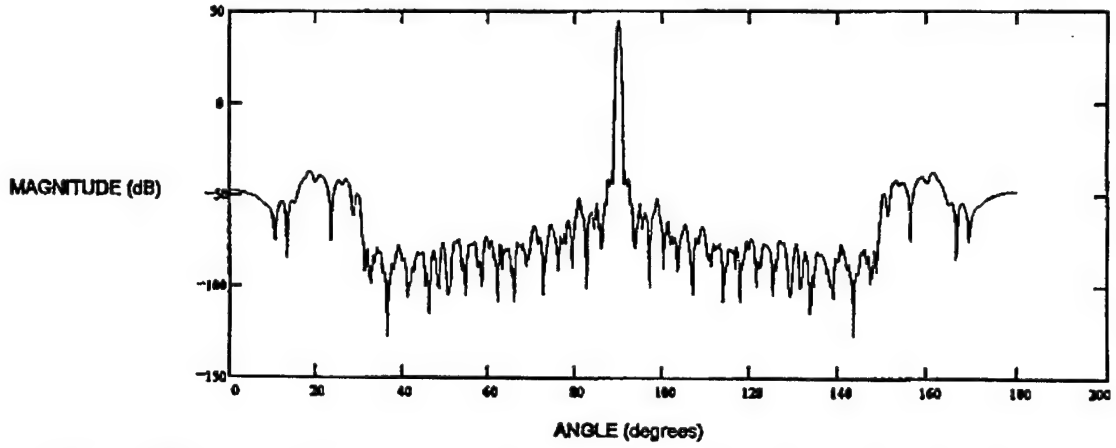

Figure 29. Product of Response and Antenna Pattern for Interpolation with Widely Random Variation and W = 20 kHz

Secondly, the band limiting operator was set to 30 kHz. The results of which can be seen in Figures 30 and 31, the ISL and PSL become 30.799 dB and 55.970 dB, respectively. The peak of the response remained at 44 dB while the side-lobes within the established band limit rose to approximately 30 dB below the main beam, which is a significant increase over the previous cases. Therefore, as was noted for the narrow variation case, the side-lobes are worse with wider interpolation bandwidth. Outside the band limit the response is equal to the uninterpolated response.

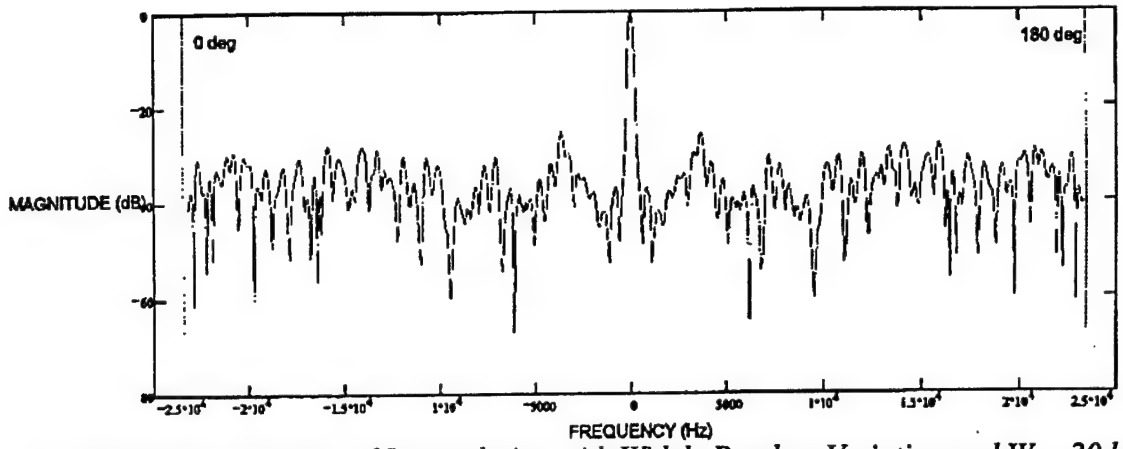

Figure 30. Frequency Response of Interpolation with Widely Random Variation and W = 30 kHz

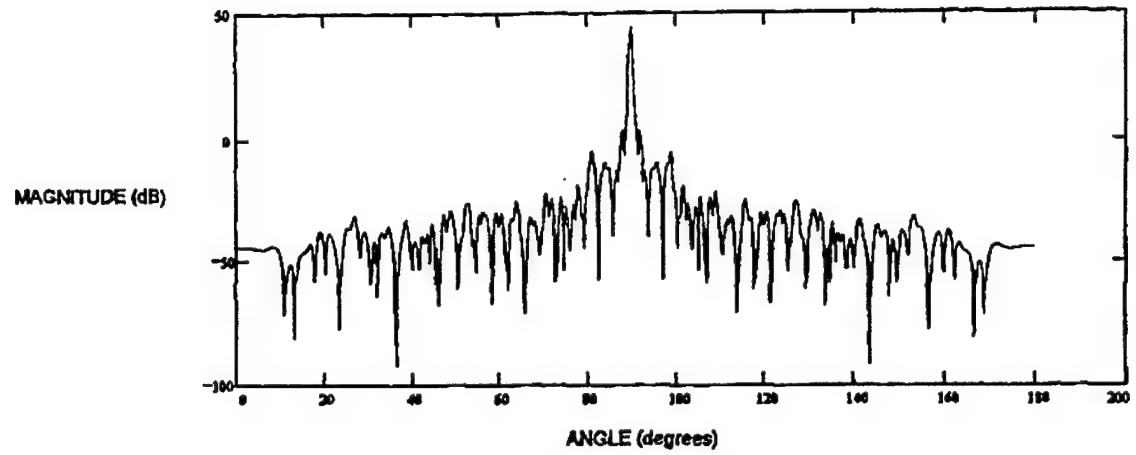

Figure 31. Product of Response and Antenna Pattern for Interpolation with Widely Random Variation and W = 30 kHz

The final analysis performed on Scenario A was to Monte Carlo one of the interpolated cases over the PRI distribution, in order to ensure that the results obtained thus far were representative of the average performance. The narrowly random variation case with a band limiting factor of 30 kHz was selected for the analysis. The frequency response of ten Monte Carlo runs is shown in Figure 32, where the curve labeled maximum is formed by taking the maximum of all the runs on a point by point basis after the interpolation has been performed. The average curve is the average of the interpolated responses on a point by point basis for all of the runs. The corresponding curves for the product of the frequency responses and the antenna pattern are shown in Figure 33.

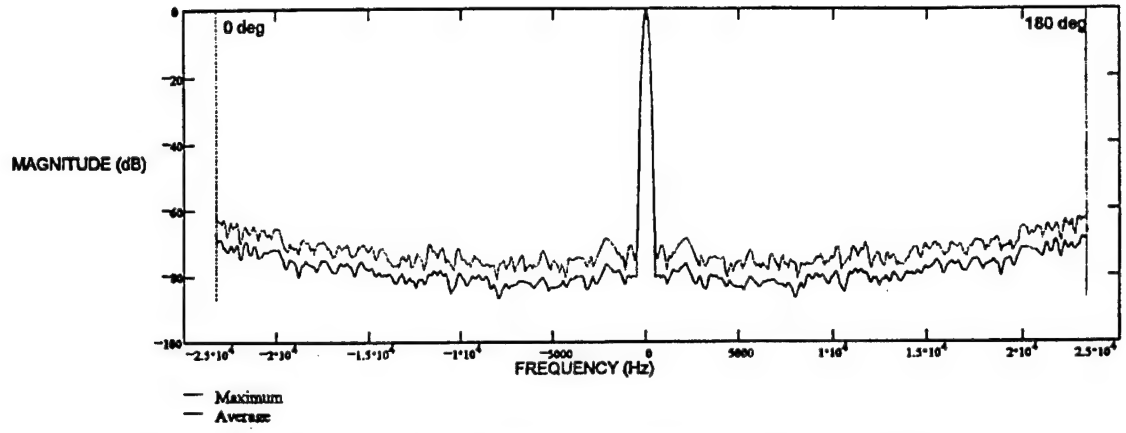

Figure 32. Monte Carloed Frequency Response of Interpolation with ±5 Percent Variation and W = 30 kHz

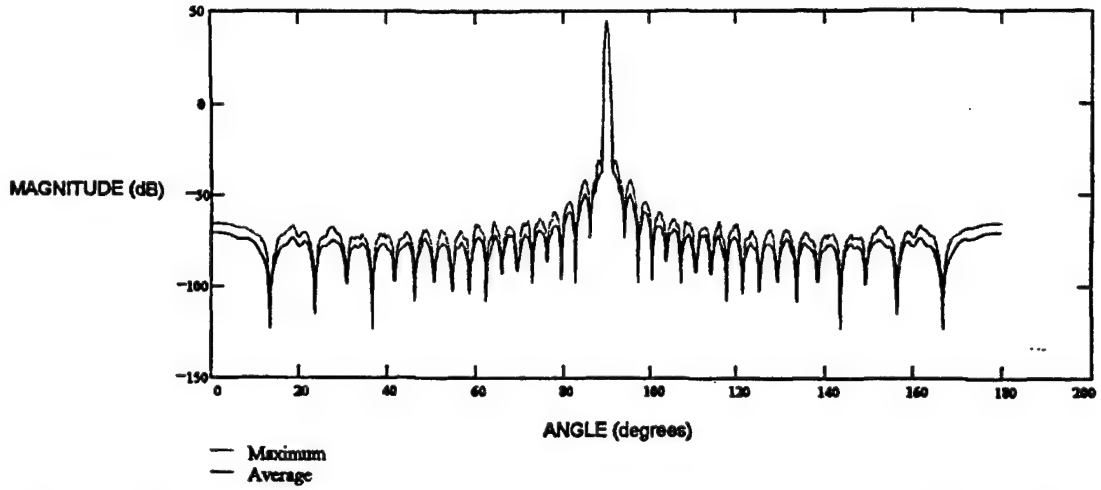

Figure 33. Product of Monte Carloed Response and Antenna Pattern of Interpolation with ±5 Percent Variation and W = 30 kHz

The ISL and PSL for the average are 68.371 dB and 83.1 dB, respectively. For the maximum the ISL was determined to be 61.64 dB and the PSL was determined to be 78.161 dB.

The initial emphasis of the analysis was placed on the system described by Scenario A, the following discussion will pertain to the results of the analysis performed on Scenario B. The first case to be examined was the uniform PRI case. This case also served as a point of comparison. Each case to be examined was weighted by a four sample Blackman-Harris Window. As before, for each case there were two figures which were of importance. The first was the weighted frequency response. The other curve of interest was the product of the frequency response and the antenna pattern. The weighted frequency response of the uniform case can be seen in Figure 34, followed by the product of the antenna pattern and the frequency response in Figure 35. The frequency response in Figure 34 appears as theoretically expected. The peak at zero has a value

equal to 33 dB, i.e. 20*log (.36*Number of pulses), where there were 128 pulses, and the side-lobes are approximately 92 dB down from the main lobe. Both the .36 factor and the -92 dB first side-lobes are characteristics of the four-sample Blackman Harris Window. Also, the Doppler ambiguities appear at multiples of the PRF as expected. The ISL and PSL for this case were determined to be 29.478 dB and 95.176 dB, respectively.

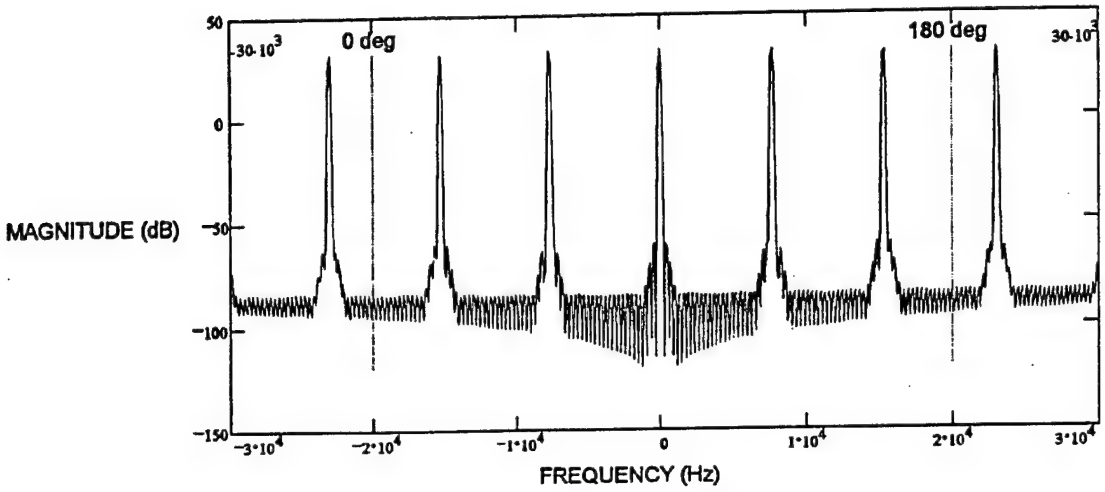

Figure 34. Frequency Response of Uniform PRF of 7.7 kHz

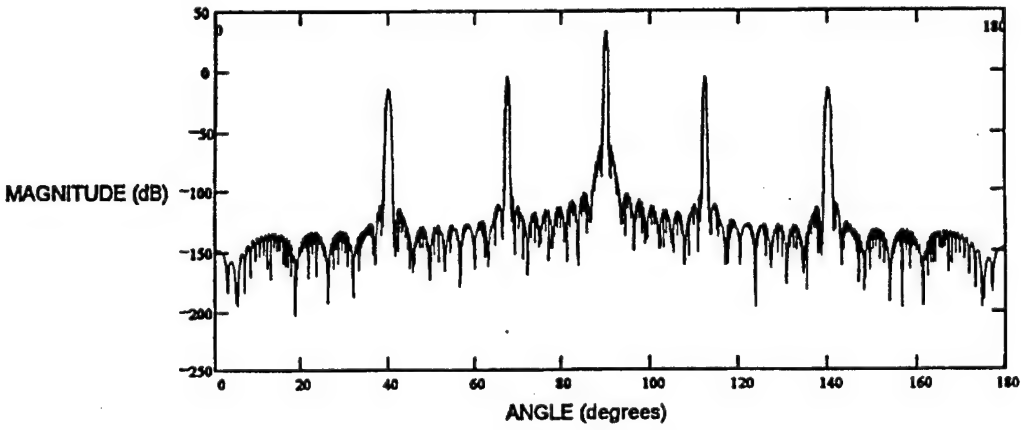

Figure 35. Product of Response and Antenna Pattern for a Uniform PRF of 7.7 kHz

The following two cases examined were the nonuniform PRI cases. Figures 36 and 37 show the curves which correspond to the narrow case i.e. ±5 percent. As was expected, the main beam has a value of approximately 33 dB as described above; however, the side-lobe structure is now different. The side-lobes now appear at approximately 42 dB below the main beam, i.e. 20*log (Number of Pulses), [2 and 8]. From Figure 36, one can also see a decrease in the magnitude of the ambiguity responses as they get farther from the main beam. However, with the narrow variation there is still a substantial response at multiples of the input frequency. The nonuniform variation is insufficient to unambiguously determine the frequency of signals at multiples of the nominal sample rate. The ISR and PSR for this case were found to be 12.229 dB and 54.489 dB, respectively.

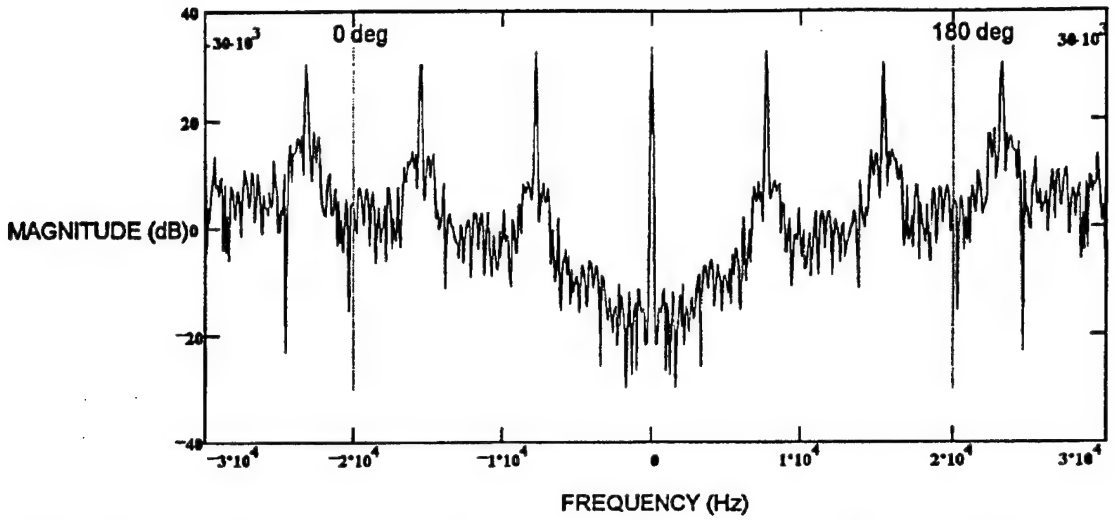

Figure 36. Frequency Response for ±5 Percent Random Variation of PRF about 7.7 kHz

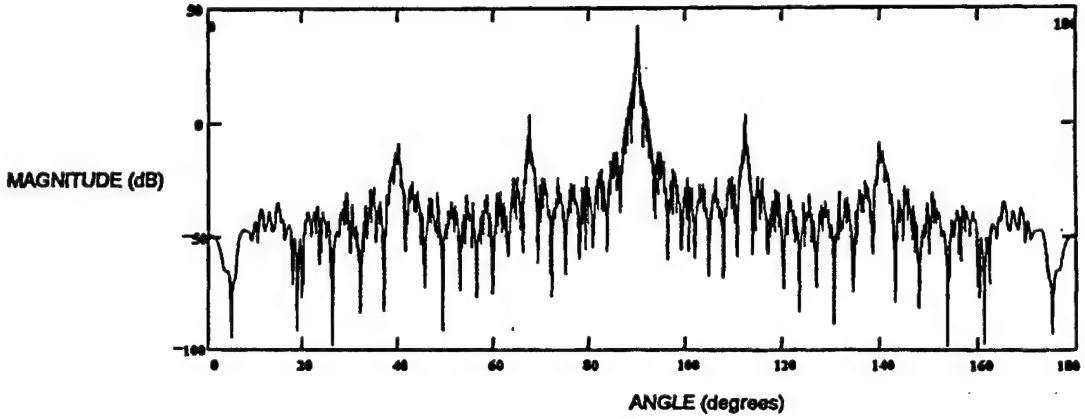

Figure 37. Product of Response and Antenna Pattern for ±5 Percent Random Variation About a PRF of 7.7 kHz

The corresponding plots for the case of wide variation are shown in Figures 38 and 39, and are shown to have an ISL of 3.936 dB and a PSL of 46.596 dB. The structure of Figure 38 is as expected with the main beam magnitude and side-lobes essentially unchanged. However, the ambiguous responses are substantially suppressed, although the side-lobes are raised. Note that the ambiguous response is still apparent at 7.7 kHz. A high degree of nonuniformity is required to totally suppress the ambiguous responses. The frequency response is poor compared to the uniform case with the same sample window.

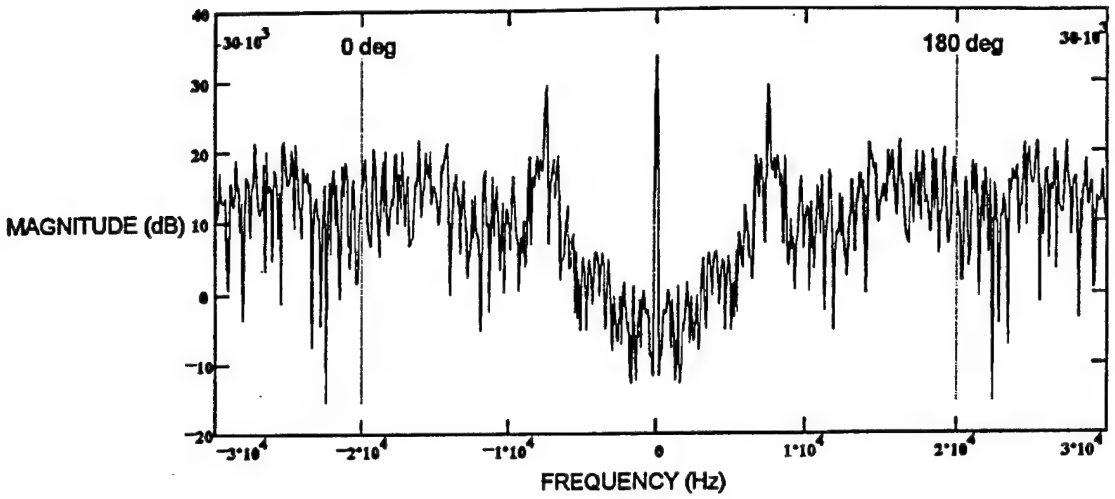

Figure 38. Frequency Response of Widely Random Variation of PRF About 7.7 kHz

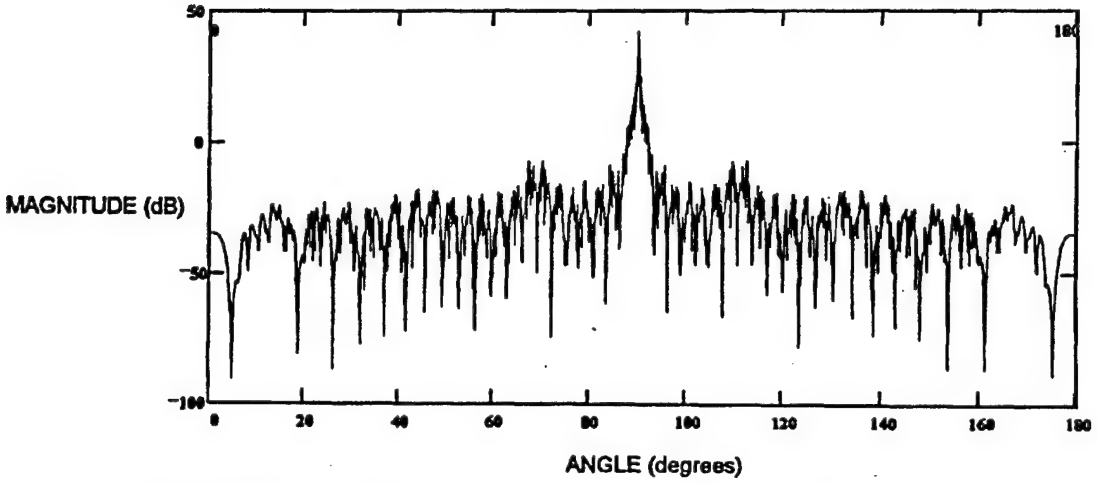

Figure 39. Product of Response and Antenna Pattern for Widely Random Variation of PRF About 7.7 kHz

The next set of configurations to be considered were the interpolated nonuniform sampled sequences. For each of the degrees of randomness the band limiting parameter was varied. Two values for this parameter were chosen to examine their effects. These values were selected to be 3 kHz and 5 kHz, for Scenario B based on the results presented in Reference 6. It was shown that performance degrades for values greater than 50 percent of the average sample rate (for I/Q sampling) [6].

In Figures 40 and 41 the effects of interpolation of a narrow random variation sequence are shown. The band limit was set to 3 kHz.

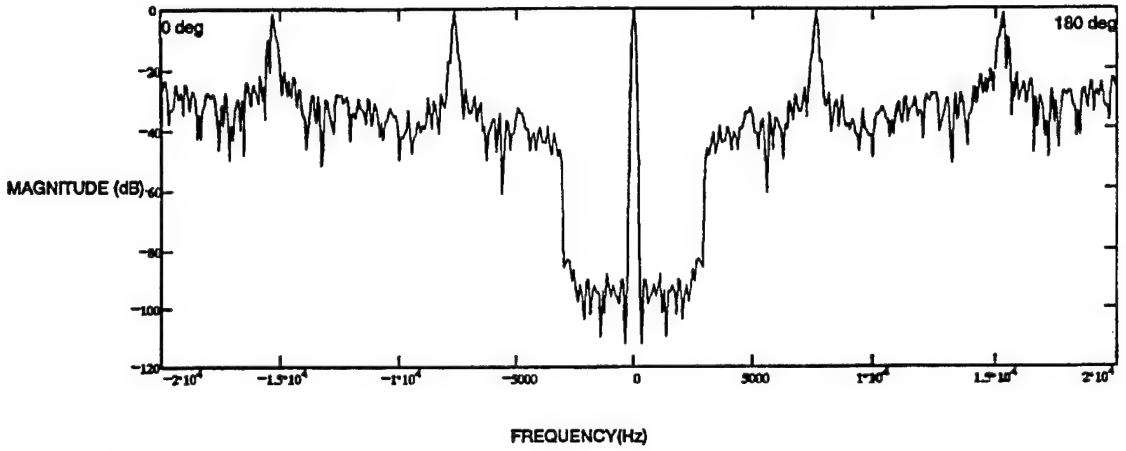

Figure 40. Frequency Response of Interpolation for the ±5 Percent Random Variation with W = 3 kHz

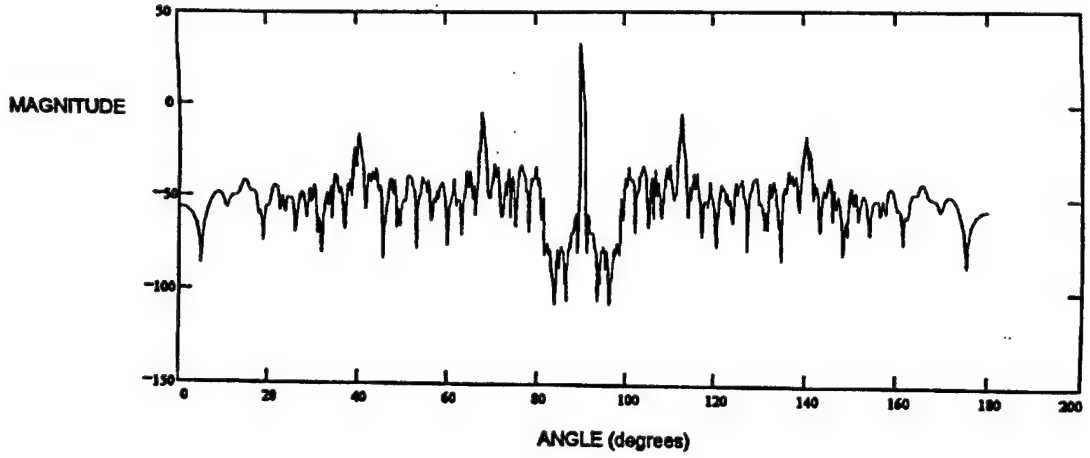

Figure 41. Product of Response and Antenna Pattern for Interpolation of ±5 Percent Random Variation with W = 3 kHz

Within the bounds of the band limit selected, the response is essentially equal to that of a uniformly sampled sequence. Outside these bounds the response behavior is similar to the uninterpolated case. The main beam had a magnitude of approximately 33 dB and the returns within the bounds of the band limiting parameter are about 92 dB below the main beam. For frequencies whose magnitude is greater than the value set for the band limit the side-lobes are less than -42 dB, which is the value determined for the side-lobes of the nonuniform uninterpolated case. The integrated side-lobe level and the peak side-lobe level were determined to be 25.729 dB and 92.445 db, respectively.

Next, the band limit was selected to be 5 kHz. These effects are plotted in Figures 42 and 43. As expected the performance showed some degradation. The side-lobes within the bounds of the band limit are somewhat higher and the response is not as distinct within the band limit as it was for the case where the band limit was 3 kHz. Outside the band limit the response is essentially the same as the uninterpolated case. The ISL for this case was determined to be 25.478 dB and while the PSL was found to be 75.985 dB.

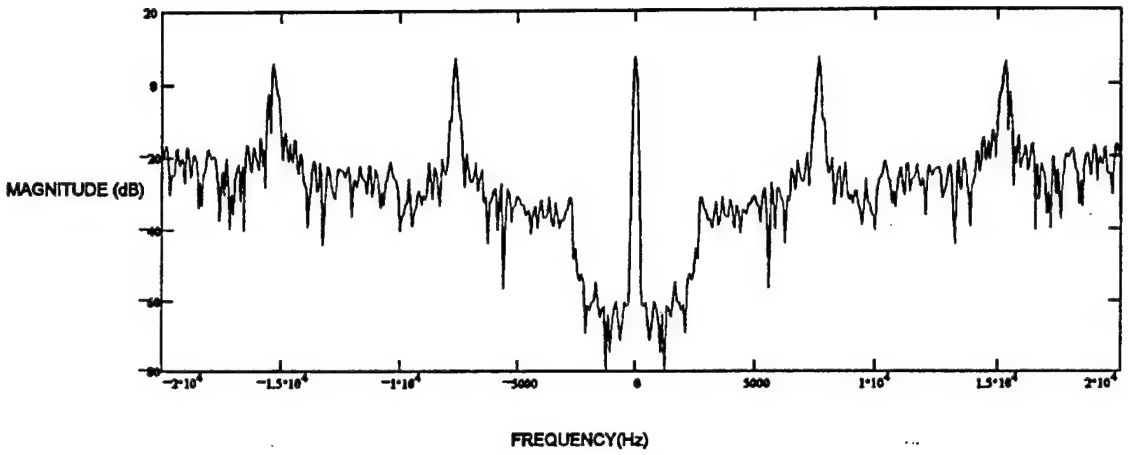

Figure 42. Frequency Response for Interpolation for ±5 Percent Random Variation About 7.7 kHz with W = 5 kHz

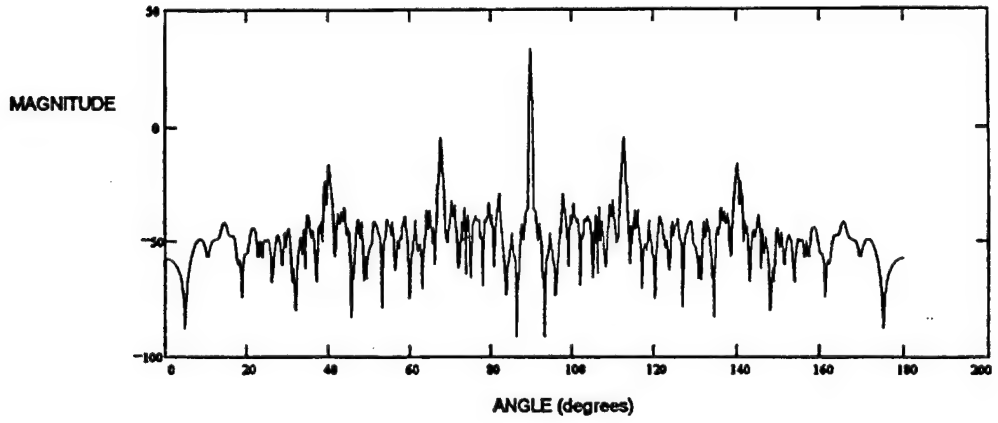

Figure 43. Product of Response and Antenna Pattern for Interpolation of ±5 Percent Random Variation with W = 5 kHz

In the plots to follow the previous two sets of results were repeated for wide sample variation. Firstly, the band limit was set to 3 kHz. These results are plotted in Figures 44 and 45. The main beam still maintains a magnitude of about 33 dB, and the side-lobes within the band limit are at approximately 80 dB down from the main beam. Outside the boundary set by the 3 kHz band limit the response is essentially equal to the uninterpolated response. The ambiguous response is suppressed in comparison with the narrow variation but the side-lobes are raised. The ISL for this case was determined to be 20.16 dB and the PSL was determined to be 84.777 dB.

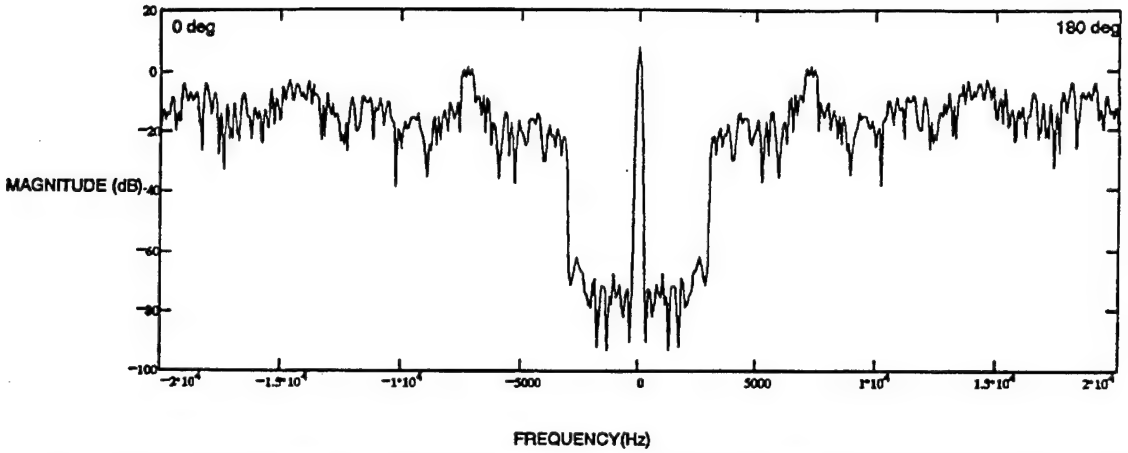

Figure 44. Frequency Response of Interpolation with Widely Random Variation and W = 3 kHz

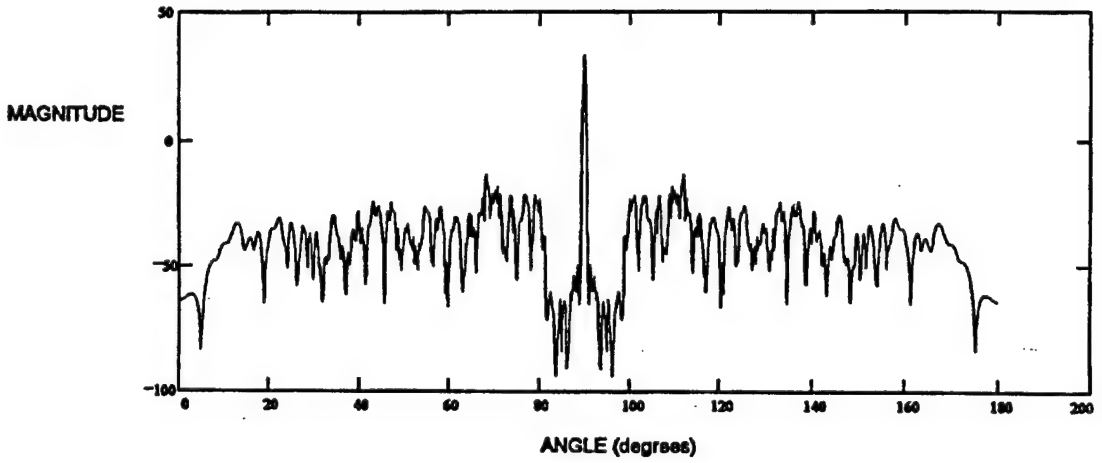

Figure 45. Product of Response and Antenna Pattern for Interpolation of Widely Random Variation and W = 3 kHz

Secondly, the band limiting operator was set to 5 kHz. The results of which can be seen in Figures 46 and 47, the ISL and PSL become 17.78 dB and 43.373 dB, respectively. The peak of the response remained at 44 dB while the side-lobes within the established band limit rose to approximately 40 dB below the main beam, which is a significant increase over the previous cases. Therefore, as was noted for the narrow variation case, the side-lobes are worse with wider interpolation bandwidth. Outside the band limit the response is equal to the uninterpolated response.

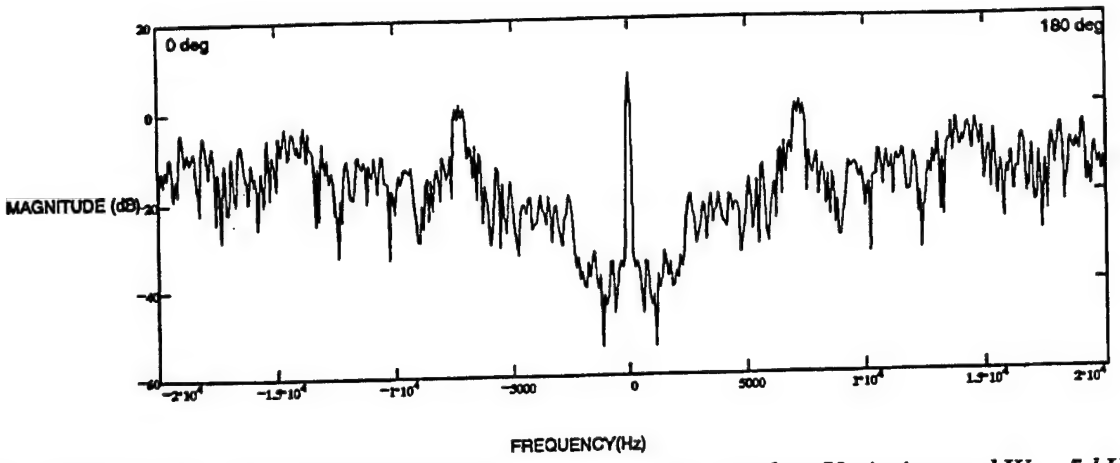

Figure 46. Frequency Response of Interpolation with Widely Random Variation and W = 5 kHz

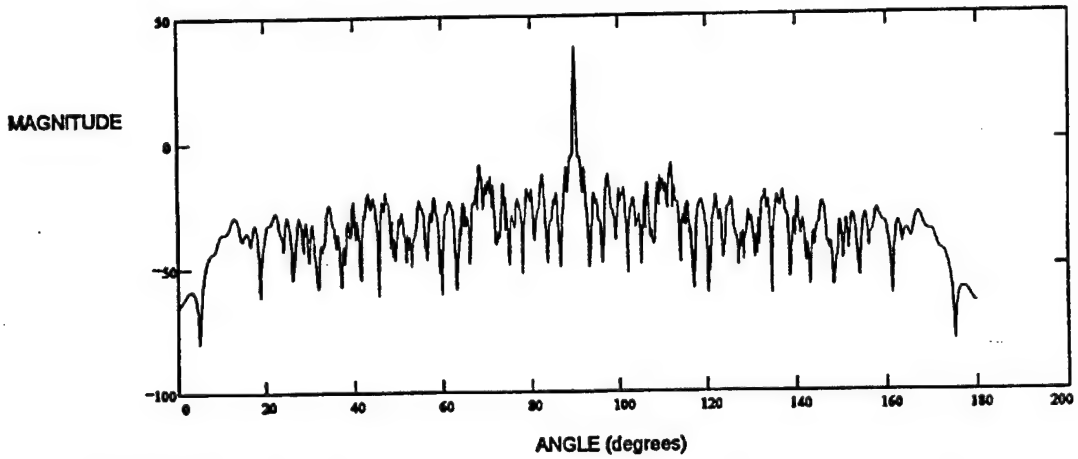

Figure 47. Product of Response and Antenna Pattern for Interpolation with Widely Random Variation and W = 5 kHz

The final analysis performed on Scenerio B was to Monte Carlo one of the interpolated cases over the PRI distribution, in order to ensure that the results obtained thus far were representative of the actual performance. The narrowly random variation case with a band limiting factor of 5 kHz was selected for the analysis. The frequency response of the Monte Carloed runs is shown in Figure 33, where the curve labeled maximum is form by taking the maximum of all the runs on a point by point basis after the interpolation has been performed. The average curve is the average of the interpolated responses on a point by point basis for all of the runs. The corresponding curves for the product of the frequency responses and the antenna pattern are shown in Figure 49.

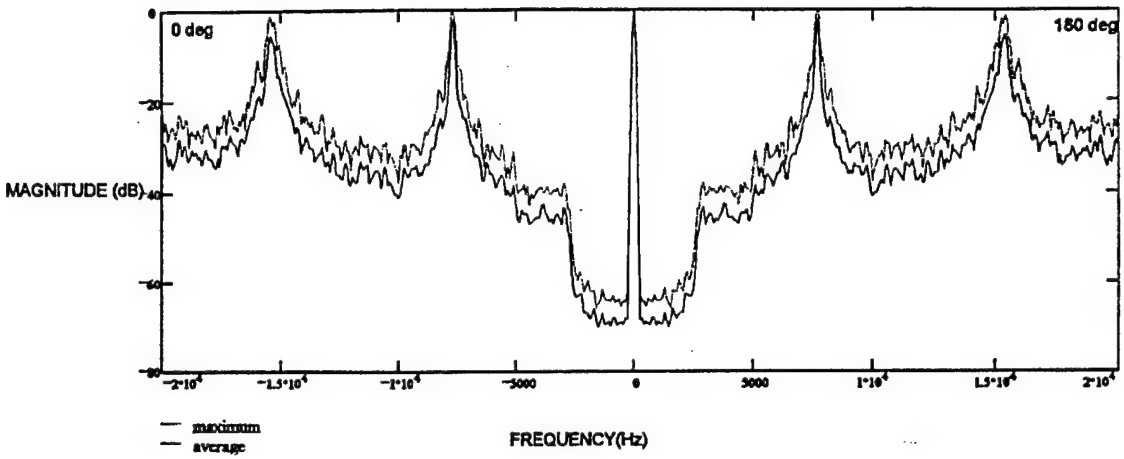

Figure 48. Monte Carloed Frequency Response of Interpolation with ±5 Percent Variation about 7.7 kHz and W = 5 kHz

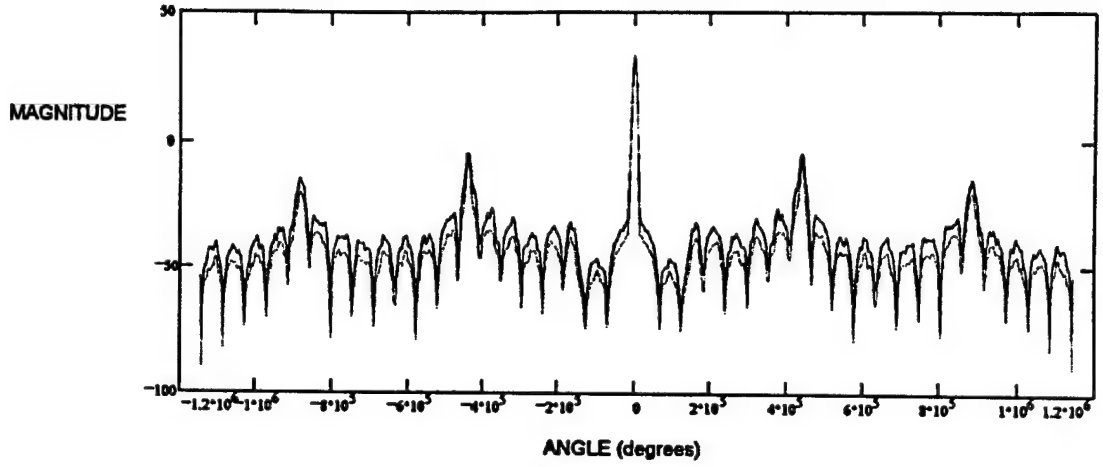

Figure 49. Product of Monte Carloed Response and Antenna Pattern of Interpolation with ±5 Percent Variation and W = 5 kHz

The ISL and PSL for the average are 68.4 dB and 83.1 dB, respectively. For the maximum the ISL was determined to be 61.6 dB and the PSL was determined to be 78.1 dB.

The responses shown in the previous figures are indicative of performance estimates of a SAR using a nonuniform PRI. All of the ISL and PSL values for the cases previously presented are summarized in Table 2.

Table 2. Summary of Processing Performance

	Scenario A		Scenerio B	
	ISL (dB)	**PSL (dB)**	**ISL (dB)**	**PSL(dB)**
Uniform	93.581	97.347	29.478	95.176
Non-Unif $\pm$5%	17.668	62.379	12.229	54.489
Non-Unif WC	10.770	48.676	3.936	46.596
Interp $\pm$5% W1	69.213 W=20kHz	96.954 W=20kHz	25.729 W=3kHz	92.455 W=3kHz
Interp $\pm$5%W2	68.663 W=30kHz	84.611 W=30kHz	25.478 W=5kHz	75.895 W=5kHz
Interp WC W1	54.724 W=20kHz	85.649 W=20kHz	20.16 W=3kHz	84.777 W=3kHz
Interp WC W2	30.799 W=30kHz	55.970 W=30kHz	17.78 W=5kHz	43.373 W=5kHz

VI. INTERPRETATION OF RESULTS

Based on the results presented in Section V it would appear that both Scenarios A and B provide comparable performance as far and the PSLs are concerned. However, the ISL vary significantly from Scenario A to Scenario B, even though in each scenario the interpolation process provides significant improvement over the nonuniform uninterpolated cases. From observation of Figures 50 through 53, the reasons for this become apparent. Figures 50 and 51 illustrate the antenna pattern and the frequency responses associated with $\pm$ 5 percent random variation and the worst case random variation, respectively, for Scenario A. Figures 52 and 53 illustrate the corresponding data for Scenario B. When comparing the figures it is obvious that the low PRF of Scenario B (7.7 kHz) is causing Doppler ambiguities to appear within the portion of the frequency response which is multiplied by the antenna pattern. The appearance of these ambiguities thus result in the large responses in the side-lobe of the product of the two curves, which leads to a smaller overall value for the ISL calculated for Scenario B than for Scenario A.

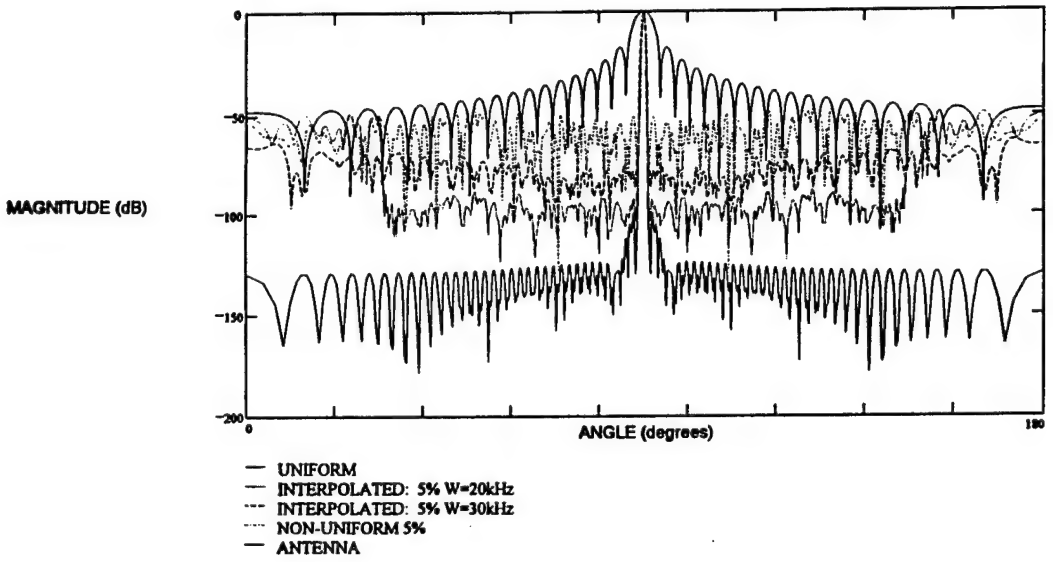

Figure 50. Antenna Pattern and Frequency Responses for Scenario A with $\pm$5 Percent Random Variation

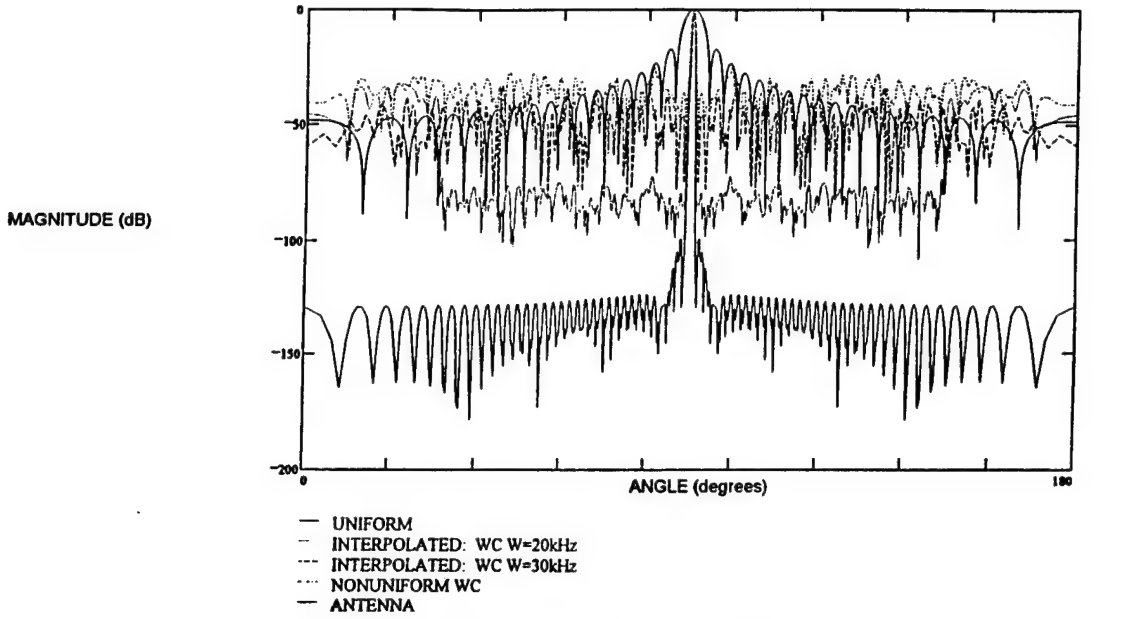

Figure 51. Antenna Pattern and Frequency Responses for Scenario A Worst Case Random Variation

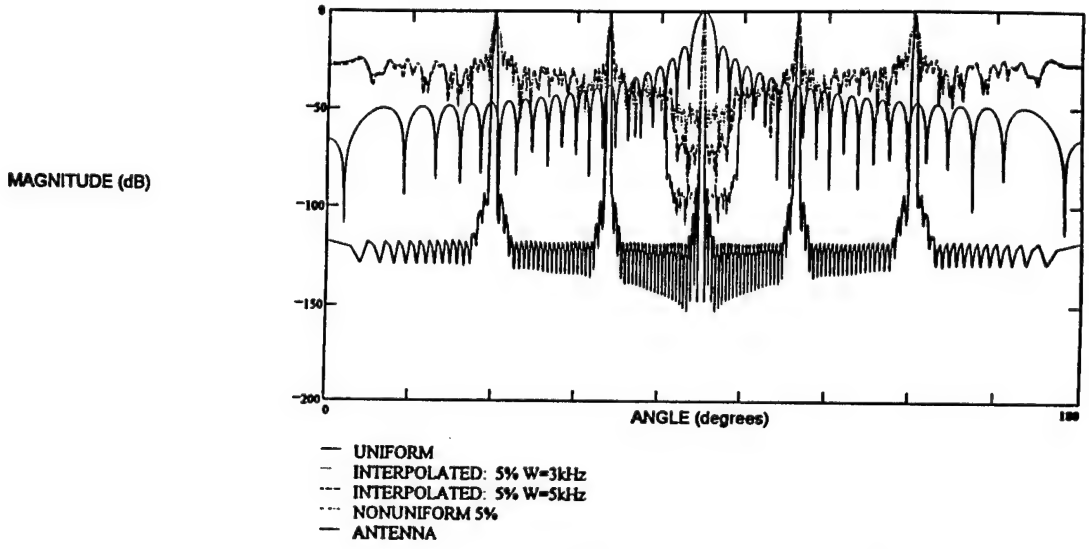

Figure 52. Antenna Pattern and Frequency Responses for Scenario B with ±5 Percent Random Variation

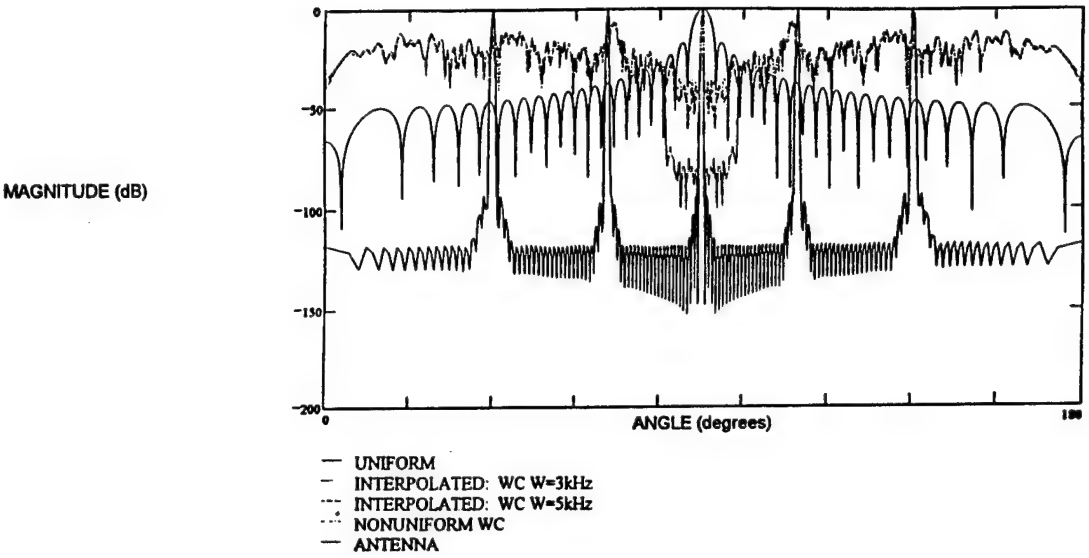

Figure 53. Antenna Pattern and Frequency Responses for Scenario B Worst Case Random Variation

The image of a SAR is basically formed from the energy contained in the main beam of the antenna. Therefore, to further understand the implications of using a low PRF radar with a nonuniform PRI to form SAR images the PSL and ISL were examined for the portion of the frequency responses which appear within the main beam of the antenna. These responses are shown in Figures 54 through 57. Figures 54 and 55 represent the responses for Scenario A with ± 5 percent random variation and worst case random variation, respectively. The corresponding responses for Scenario B are shown in Figures 56 and 57.

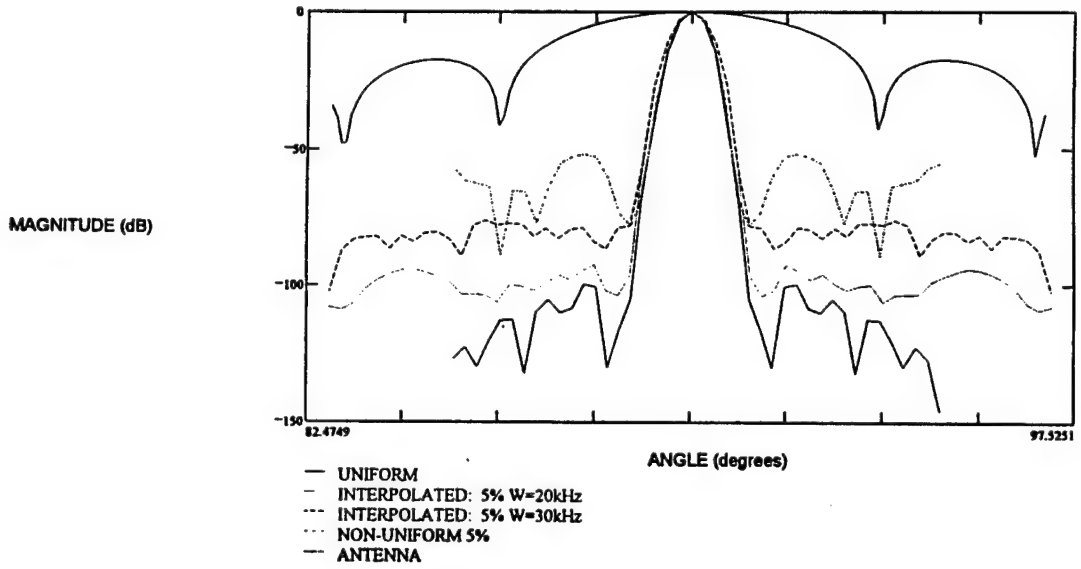

Figure 54. Main Beam of Antenna Pattern and Corresponding Frequency Responses for Scenario A ± 5 Percent Random Variation

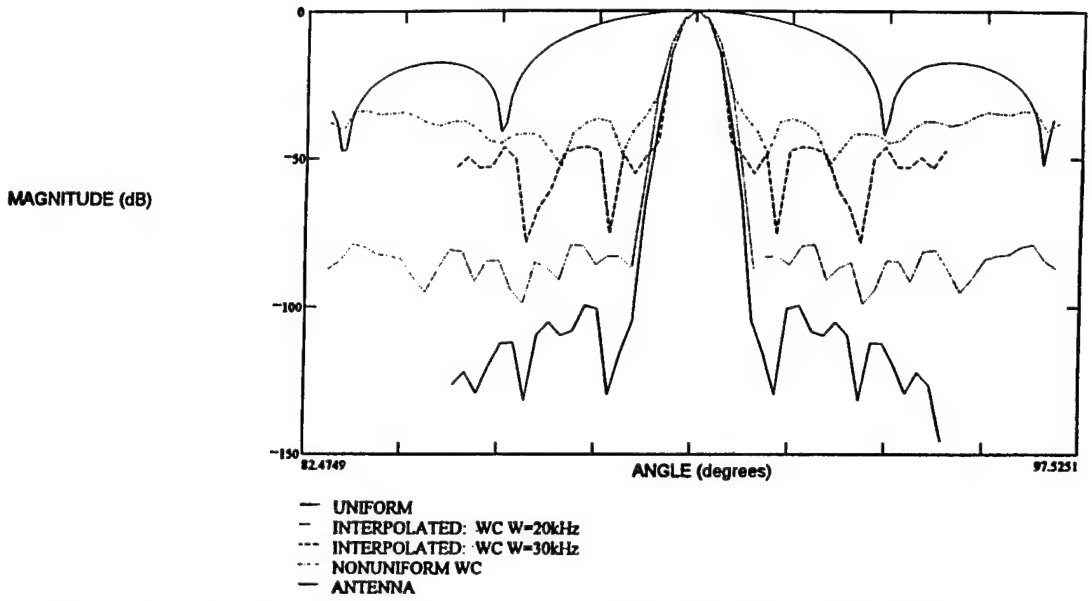

Figure 55. Main Beam of Antenna Pattern and Corresponding Frequency Responses for Scenario A Worst Case Random Variation

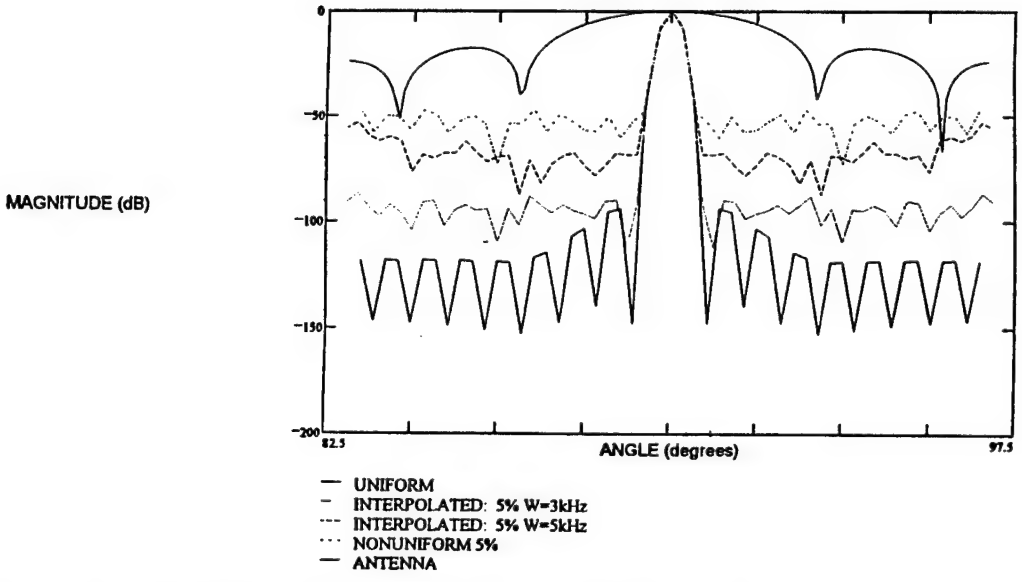

Figure 56. Main Beam of Antenna Pattern and Corresponding Frequency Responses for Scenario B ±5 Percent Random Variation

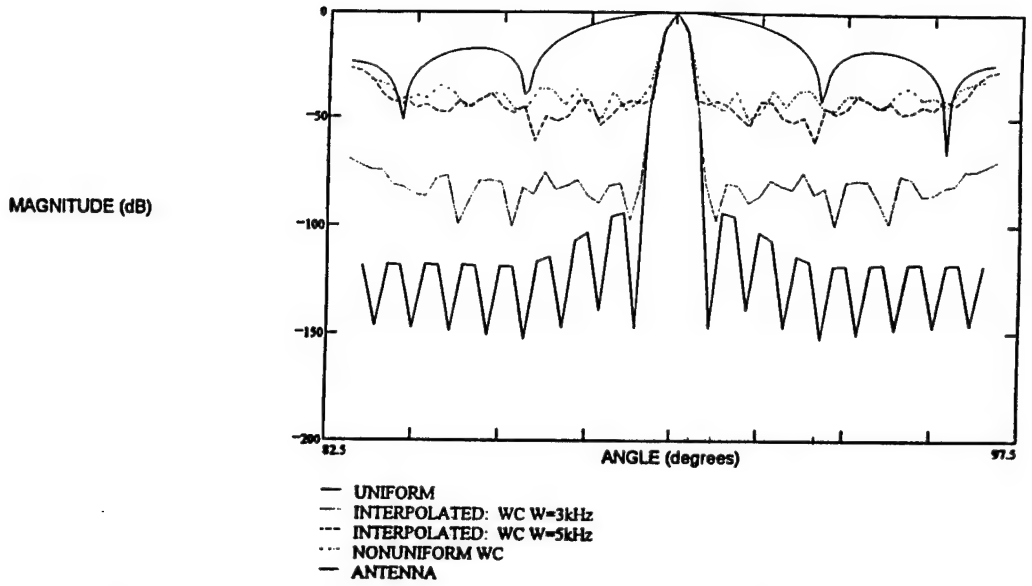

Figure 57. Main Beam of Antenna Pattern and Corresponding Frequency Responses for Scenario B Worst Case Random Variation

From the figures the PSL values that were calculated from the data are easily verified by observation of the side-lobe levels of the frequency responses and the corresponding level of the antenna pattern and adding the two values. The ISL values for the antenna main beam portion, ISL_{MB} of the responses were calculated and are shown in Table 3, along with the previously calculated ISL values when all of the side-lobes from 0 to 180 degrees were considered.

From these values it can be seen that the ISL_{MB} values for Scenario B are more comparable with those calculated for Scenario A. Where were only two cases in Scenario A where there was a significant change in the ISL and ISL_{MB} values, these were the cases where interpolation was performed and the band limit was less than 50 percent of the average PRF. This is due to the increase in the frequency response at frequencies greater than the band limit, which were not considered in the ISL calculation for the antenna main beam.

Table 3. Summary of Waveform Performance for Entire Antenna Pattern and Main Beam Antenna Pattern

	Scenario A		Scenerio B	
	ISL (dB)/ISL_{MB} (dB)	PSL (dB)	ISL (dB)/ISL_{MB} (dB)	PSL(dB)
Uniform	93.581 / 94.042	97.347	29.478 / 90.309	95.176
Non-Unif ±5%	17.668 / 17.668	62.379	12.229 / 15.549	54.489
Non-Unif WC	10.770 / 10.770	48.676	3.936 / 6.153	46.596
Interp ±5% W1	69.213 / 93.097 W=20kHz	96.954 W=20kHz	25.729 / 84.756 W=3kHz	92.455 W=3kHz
Interp ±5%W2	68.663 / 75.483 W=30kHz	84.611 W=30kHz	25.478 / 61.177 W=5kHz	75.895 W=5kHz
Interp WC W1	54.724 / 76.643 W=20kHz	85.649 W=20kHz	20.16 / 71.55 W=3kHz	84.777 W=3kHz
Interp WC W2	30.799 / 35.615 W=30kHz	55.970 W=30kHz	17.78 / 33.402 W=5kHz	43.373 W=5kHz

VII. CONCLUSIONS

From the data presented it can be seen that there are significant improvements to be had by choosing to use the interpolation based filter approach for a nonuniform PRI waveform as opposed to using the nonuniform uninterpolated waveform. The interpolation approach provides significantly higher ISL and PSL over the noninterpolated cases.

In general, Scenario B has lower ISL values compared to Scenario A because of the PRF frequency. The lower PRF causes more Doppler ambiguities to appear in the frequency span which is transformed into angular coordinates to perform the multiplication with the antenna pattern. However, based on the fact that a SAR essentially uses the energy returning from the main beam of the antenna to form the image there is little difference in the ISL_{MB} values calculated for Scenarios A and B.

For the data presented it is easily shown that an interpolation based filter provides significant improvement in ISL and PSL over a standard nonuniform PRI waveform, with performance approaching the uninterpolated cases as the degree of randomness of the PRI increases. Therefore, provided the system is sensitive enough to withstand the loss in signal-to-interference associated with the processing, it would be feasible to implement a SAR with a nonuniform PRI.

REFERENCES

1. Maier, Mark W., Non-Uniform PRI Pulse-Doppler Radar, IEEE Southeastern Symposium on System Theory, IEEE Computer Society Press, p. 164-168, 1993.

2. Maier, Mark W., Airborne Clutter Performance of Randomized Radar Waveforms, Ph.d. Dissertation, Univ. of Southern California, 1991.

3. Morris, Guy V.: "Airborne Pulsed Doppler Radar", Artech House, Norwood, MA, 1988.

4. Curlander, John C. and McDonough, Robert N.: "Synthetic Aperture Radar: Systems and Signal Processing", Wiley and Sons, New York, NY, 1991.

5. Kirk, Jr., J. C.: "Digital Synthetic Aperture Radar Technology," *Record of the IEEE 1975 International Radar Conference,* Arlington, VA, pp. 482-487, 21-23 April 1975.

6. Hovanessian S. A., "Introduction to Synthetic Array and Imaging Radars", Artech House, Dedham, MA, 1980.

7. Wehner, Donald R., "High Resolution Radar", Artech House, Norwood, MA, 1987.

8. Brookner, Eli, "Radar Technology", Artech House, Bedham, MA, 1977.

9. Stimson, G. W., "Introduction to Airborne Radar", Hughes Aircraft Company, El Segundo, CA, 1983.

10. Rihaczek, A. W., "Principles of High Resolution Radar", McGraw-Hill, New York, NY, 1969.

11. Harris, F. J., *On The Use of Windows for Harmonic Analysis with Discrete Fourier Transform,* Proceedings of the IEEE, Vol 66 (1), 51-83, January 1978.

LIST OF SYMBOLS

Symbol	Definition
a_{qp}	the qp element of A^{-1}
A	Matrix used to perform interpolation
α	Depression angle of antenna
c	Speed of light
C_R	Complex voltage determined from system parameters and range bin
D	Diameter of antenna
ΔAZ	Theoretical Limit of Azimuth Resolution
Δf	Frequency bandwidth of digital filter
Δf_i	Attainable frequency resolution of signal processing equipment
$(\Delta f)_L$	Maximum frequency excursion
ΔR	Slant range resolution
ΔR_x	Down range resolution
ΔR_y	Cross-range resolution
$\Delta\Theta$	Angle between points A and B
f_A	Doppler shift at point A
f_B	Doppler shift at point B
f_d	Doppler frequency
f_o	Frequency of transmitted radar signal
f_r	Frequency of returned signal
ϕ_r	Phase of returned signal
γ	Half-Power beamwidth
l	Actual antenna length
l_1	Cross-range dimension of antenna
L	Synthetic array length
λ	Wavelength
N	Total number of samples
N_D	Number of samples per range bin
N_r	Number of range gates

LIST OF SYMBOLS (cont)

Symbol	Definition
PRF	Pulse Repetition Frequency
Θ	Cant angle of the radar
Θ_{BW}	3 dB Antenna Beamwidth
R	Range
R'	Target's closing/opening rate in direction of R
R_o	Initial range
R_{max}	Maximum measurable range
s_k	Sample corresponding to k^{th} pulse
S(f)	Fourier transform of interpolated sequence
t	Time
t_M	Sample time for the M^{th} nonuniformly sampled pulse
T	Pulse repetition interval
T_k	Time to k^{th} inter pulse interval
T_{acq}	Data acquisition time
τ	Transmitted pulse duration
V	Velocity
V_r	Returned signal
V_t	Transmitted radar signal
w	Weighting function
W	Bandwidth over which interpolator assumes signals are present
W_r	Receiver bandwidth
WC	Worst case random variation
X_{ME}	Minimum energy band limited interpolator

APPENDIX A
PARAMETERS FOR SCENARIO A

APPENDIX A
PARAMETERS FOR SCENARIO A

RANGE: $R := 2 \cdot 10^3$

FREQUENCY: $f := 35000 \cdot 10^6$ MHz

ANTENNA DIMENSIONS: $l_1 := .152$ m

$l_2 := .152$ m

ANTENNA EFFICIENCY: $nu := .7$

SPEED OF LIGHT: $c := 3 \cdot 10^8$ m/sec

WAVELENGTH: $\lambda := \frac{c}{f}$ $\lambda = 0.0086$

ANTENNA GAIN: $G := \frac{4 \cdot \pi \cdot l_1 \cdot l_2 \cdot nu}{\lambda^2}$ $G = 2.781 \cdot 10^3$

BEAMWIDTH: $BW_R := \frac{\lambda}{l_1}$ $BW_R = 0.056$

$BW_A := \frac{\lambda}{l_2}$ $BW_A = 0.056$

ANGLE OFF VELOCITY VECTOR: $\Theta := 90$

DEPRESSION ANGLE: $\alpha := 30$

HEIGHT OF PLATFORM: $H := R \cdot \cos\left[(90 - \alpha) \cdot \frac{\pi}{180}\right]$ $H = 1 \cdot 10^3$

SWATH WIDTH: $SW := \frac{R \cdot \lambda}{l_1 \cdot \sin\left(\alpha \cdot \frac{\pi}{180}\right)}$ $SW = 224.972$

SWATH LENGTH: $SL := \frac{R \cdot \lambda}{l_2}$ $SL = 112.486$

RANGE TO FRONT OF SW: $R_1 := \frac{H}{\cos\left[\left[90 - \alpha - BW_R \cdot \left(\frac{180}{2 \cdot \pi}\right)\right] \cdot \frac{\pi}{180}\right]}$ $R_1 = 1.908 \cdot 10^3$

RANGE TO BACK OF SW: $R_N := \frac{H}{\cos\left[\left[(90 - \alpha) + BW_R \cdot \left(\frac{180}{2 \cdot \pi}\right)\right] \cdot \frac{\pi}{180}\right]}$ $R_N = 2.103 \cdot 10^3$

VELOCITY: $V := 100$ m/sec

TIME TO FLY 1 BEAMWIDTH: $T_b := \frac{SL}{V}$ $T_b = 1.125$

TOTAL FREQ. SPREAD (Az BW): $\Delta f_d := \frac{2 \cdot V}{l_2}$ $\Delta f_d = 1.312 \cdot 10^3$

PULSE WIDTH: $\tau := 1.0 \cdot 10^{-6}$ sec

RANGE RESOLUTION: (w/o pulse compression) $\Delta R_x := \left| \frac{c \cdot \tau}{2 \cdot \cos\left[\alpha \cdot \left(\frac{\pi}{180}\right)\right]} \right|$ $\Delta R_x = 173.205$

DESIRED RANGE RESOL.: $\Delta R_{xc} := 10\,m$

PULSE COMPRESSION RATIO: $D := \frac{\Delta R_x}{\Delta R_{xc}}$ $D = 17.321$

P. COMP. FREQ EXCURSION: $\Delta := \frac{D}{\tau}$ $\Delta = 1.732 \cdot 10^7$

SAMPLING RATE (NYQUIST): $SR := 2 \cdot \Delta$ $SR = 3.464 \cdot 10^7$

NO. OF RANGE GATES: $N_r := \frac{SW}{\Delta R_{xc}}$ $N_r = 22.497$

COMPRESSED P. WIDTH: $\tau_c := \frac{\tau}{D}$ $\tau_c = 5.774 \cdot 10^{-8}$

TIME EQUIV OF Nr R. GATES $T_s := N_r \cdot \tau_c$ $T_s = 1.299 \cdot 10^{-6}$

NO. OF SAMPLES: $N_s := T_s \cdot SR$ $N_s = 44.994$

AZIMUTH RESOLUTION DESIRED $\Delta R_y := 10m$

THEORETICAL ANTENNA DIA: $Dia := \Delta R_y \cdot 2$ $Dia = 20$

FILTER FREQ. BANDWIDTH: $\Delta f_i := \frac{Dia \cdot V \cdot \sin\left(\Theta \cdot \frac{\pi}{180}\right)}{\lambda \cdot R}$ $\Delta f_i = 116.667$

FILTER TIME CONSTANT: (coherent integration time) $T_c := \frac{1}{\Delta f_i}$ $T_c = 0.009$

PULSE REPETITION FREQ. REQ: $PRF_{min} := \Delta f_d$ $PRF_{min} = 1.312 \cdot 10^3$

$PRF_{max} := \frac{c}{2 \cdot R_N}$ $PRF_{max} = 7.132 \cdot 10^4$

DEFINITION OF PRF INTERVAL: 40kHz < PRF < 73kHz

$PRF_{min} := 2 \cdot \frac{V}{\lambda} \cdot \cos\left(\alpha \cdot \frac{\pi}{180}\right) \cdot 2$ $PRF_{min} = 4.041 \cdot 10^4$

$PRF_{max} := PRF_{max}$ $PRF_{max} = 7.132 \cdot 10^4$

NOMINAL PRF: $PRF := \frac{PRF_{max} + PRF_{min}}{2}$ $PRF = 5.587 \cdot 10^4$

PRI INTERVAL: $PRI_{max} := \frac{1}{PRF_{min}}$ $PRI_{max} = 2.474 \cdot 10^{-5}$

$PRI_{min} := \frac{1}{PRF_{max}}$ $PRI_{min} = 1.402 \cdot 10^{-5}$

NOMINAL PRI: $PRI := \frac{1}{PRF}$ $PRI = 1.79 \cdot 10^{-5}$

DEFINITION OF PRI: 14.0 usec. < PRI < 21.43 usec.

NO. PULSES COH. INTEG: $N_p := T_c \cdot PRF$ $N_p = 479$

SYNTHETIC ARRAY LENGTH: $L := V \cdot T_c$ $L = 0.857$

NO. OF FILTERS/ RG FOR Tc: $N_f := \frac{L}{\left(\frac{Dia}{2}\right)}$ $N_f = 0.086$

TOT. NO. OF FILTERS IN SL: $N_d := \frac{SL}{\left(\frac{Dia}{2}\right)}$ $N_d = 11.249$

NO. OF INDEP. LOOKS/ : GROUND RESOL. CELL $Looks := \frac{N_d}{N_f}$ $Looks = 131.234$

APPENDIX B
PARAMETERS FOR SCENARIO B

APPENDIX B
PARAMETERS FOR SCENARIO B

RANGE: $R := 10 \cdot 10^3$

FREQUENCY: $f := 10 \cdot 10^9$ Hz

ANTENNA DIMENSIONS: $l_1 := .609$ m

$l_2 := .609$ m

ANTENNA EFFICIENCY: $nu := .7$

SPEED OF LIGHT: $c := 3 \cdot 10^8$ m/sec

WAVELENGTH: $\lambda := \frac{c}{f}$ $\lambda = 0.03$

ANTENNA GAIN: $G := \frac{4 \cdot \pi \cdot l_1 \cdot l_2 \cdot nu}{\lambda^2}$ $G = 3.632 \cdot 10^3$

BEAMWIDTH: $BW_R := \frac{\lambda}{l_1}$ $BW_R = 0.049$

$BW_A := \frac{\lambda}{l_2}$ $BW_A = 0.049$

ANGLE OFF VELOCITY VECTOR: $\Theta := 90$

DEPRESSION ANGLE: $\alpha := 30$

HEIGHT OF PLATFORM: $H := R \cdot \cos\left[(90 - \alpha) \cdot \frac{\pi}{180}\right]$ $H = 5 \cdot 10^3$

SWATH WIDTH: $SW := \frac{R \cdot \lambda}{l_1 \cdot \sin\left(\alpha \cdot \frac{\pi}{180}\right)}$ $SW = 984.252$

SWATH LENGTH: $SL := \frac{R \cdot \lambda}{l_2}$ $SL = 492.126$

RANGE TO FRONT OF SW: $R_1 := \frac{H}{\cos\left[\left[90 - \alpha - BW_R \cdot \left(\frac{180}{2 \cdot \pi}\right)\right] \cdot \frac{\pi}{180}\right]}$ $R_1 = 9.594 \cdot 10^3$

RANGE TO BACK OF SW: $R_N := \frac{H}{\cos\left[\left[(90 - \alpha) + BW_R \cdot \left(\frac{180}{2 \cdot \pi}\right)\right] \cdot \frac{\pi}{180}\right]}$ $R_N = 1.045 \cdot 10^4$

VELOCITY: $V := 300$ m/sec

TIME TO FLY 1 BEAMWIDTH: $T_b := \frac{SL}{V}$ $T_b = 1.64$

TOTAL FREQ. SPREAD (Az BW): $\Delta f_d := \frac{2 \cdot V}{l_2}$ $\Delta f_d = 984.252$

PULSE WIDTH: $\tau := 1.0 \cdot 10^{-6}$ sec

RANGE RESOLUTION: (w/o pulse compression) $\Delta R_x := \left| \frac{c \cdot \tau}{2 \cdot \cos\left[\alpha \cdot \left(\frac{\pi}{180}\right)\right]} \right|$ $\Delta R_x = 173.205$

DESIRED RANGE RESOL.: $\Delta R_{xc} := 30\,m$

PULSE COMPRESSION RATIO: $D := \frac{\Delta R_x}{\Delta R_{xc}}$ $D = 5.774$

P. COMP. FREQ EXCURSION: $\Delta := \frac{D}{\tau}$ $\Delta = 5.774 \cdot 10^6$

SAMPLING RATE (NYQUIST): $SR := 2 \cdot \Delta$ $SR = 1.155 \cdot 10^7$

NO. OF RANGE GATES: $N_r := \frac{SW}{\Delta R_{xc}}$ $N_r = 32.808$

COMPRESSED P. WIDTH: $\tau_c := \frac{\tau}{D}$ $\tau_c = 1.732 \cdot 10^{-7}$

TIME EQUIV OF Nr R. GATES $T_s := N_r \cdot \tau_c$ $T_s = 5.683 \cdot 10^{-6}$

NO. OF SAMPLES: $N_s := T_s \cdot SR$ $N_s = 65.617$

AZIMUTH RESOLUTION DESIRED $\Delta R_y := 30m$

THEORETICAL ANTENNA DIA: $Dia := \Delta R_y \cdot 2$ $Dia = 60$

FILTER FREQ. BANDWIDTH: $\Delta f_i := \frac{Dia \cdot V \cdot \sin\left(\Theta \cdot \frac{\pi}{180}\right)}{\lambda \cdot R}$ $\Delta f_i = 60$

FILTER TIME CONSTANT: (coherent integration time) $T_c := \frac{1}{\Delta f_i}$ $T_c = 0.017$

PULSE REPETITION FREQ. REQ: $PRF_{min} := \Delta f_d$ $PRF_{min} = 984.252$

$PRF_{max} := \frac{c}{2 \cdot R_N}$ $PRF_{max} = 1.436 \cdot 10^4$

DEFINITION OF PRF INTERVAL: 1kHz < PRF < 14.36kHz

$PRF_{min} := 1 \cdot 10^3$ $PRF_{min} = 1 \cdot 10^3$

$PRF_{max} := PRF_{max}$ $PRF_{max} = 1.436 \cdot 10^4$

NOMINAL PRF: $PRF := \frac{PRF_{max} + PRF_{min}}{2}$ $PRF = 7.678 \cdot 10^3$

PRI INTERVAL: $PRI_{max} := \frac{1}{PRF_{min}}$ $PRI_{max} = 0.001$

$PRI_{min} := \frac{1}{PRF_{max}}$ $PRI_{min} = 6.966 \cdot 10^{-5}$

NOMINAL PRI: $PRI := \frac{1}{PRF}$ $PRI = 1.302 \cdot 10^{-4}$

DEFINITION OF PRI: 69.6 usec. < PRI < 100 usec.

NO. PULSES COH. INTEG: $N_p := T_c \cdot PRF$ $N_p = 128$

SYNTHETIC ARRAY LENGTH: $L := V \cdot T_c$ $L = 5$

NO. OF FILTERS/ RG FOR Tc: $N_f := \frac{L}{\left(\frac{Dia}{2}\right)}$ $N_f = 0.167$

TOT. NO. OF FILTERS IN SL: $N_d := \frac{SL}{\left(\frac{Dia}{2}\right)}$ $N_d = 16.404$

NO. OF INDEP. LOOKS/ : GROUND RESOL. CELL $Looks := \frac{N_d}{N_f}$ $Looks = 98.425$

INITIAL DISTRIBUTION LIST

	Copies
IIT Research Institute ATTN: GACIAC 10 W. 35th Street Chicago, IL 60616	1
Commander U. S. Army Laboratory Command Harry Diamond Laboratories ATTN: SLCHD-RT-AC/Dr. J. Nemarich 2800 Powder Mill Rd. Adelphi, MD 20783	1
Commander U. S. Army Communications Electronics Command Night Vision and Electro-Optics Command Ft. Belvoir, VA 22062	1
Commander U. S. Army AMSAA ATTN: AMXSY-MP AMXSY-GS, Mr. Marty Perry, Aberdeen Proving Ground, MD 21005-5071	1 1
Commander Armament Division ATTN: AD/YNJ Eglin AFB, FL 32542-5000	2
AFALT/SAI ATTN: Mr. C. Coker Eglin AFB, 32579	1
AFALT/CCN ATTN: Dr. Sam Lambert Eglin AFB, FL 32542-5434	1
Commander U. S. Army Survivability MGT Office ATTN: SLCSM-D 2800 Powder Mill Road Adelphi, MD 20783-1145	1

INITIAL DISTRIBUTION LIST (cont.)

	Copies
Commander U. S. Army Vulnerability Assessment Laboratory ATTN: SLCVA-GCF/Mr.L. Anderson White Sands Missile Range, NM 88002-5513	1
Headquarters ATTN: DAMA-ER, COL, M. Gray (Room 2E360, Pentagon) Washington, DC 20210-0620	1
Commander U. S. Army AMCDE-SM/Mr. Berg 5001 Eisenhower Blvd. Alexandria, VA 22333-001	2
Commander Defense Advanced Research Projects Agency ATTN: TTO/Mr. Hafer 1400 Wilson Blvd. Arlington, VA 22209	1
Commander U. S. Army ARDEC ATTN: SMCAR-FS, Dr. Davidson SMCAR-FSP, Mr.Zimpo SMCAR-FSP-IS, Ms. Dibble SMCAR-FSP-E, Mr. Goldfarb Mr. Ericson Picatinny Arsenal, NJ 07806-5000	1 1 1 1 1
Commander U. S. Army Aviation R&D Command P. O. Box 209 St. Louis, MO 63166	1
Commander ASAARTA (AVSCOM) ATTN: SAVRT-TY-PM, Mr. Shostak Ft Eustis, VA 23604-5577	1

INITIAL DISTRIBUTION LIST (cont.)

		Copies
Commander U .S. Army Ballisic Research Laboratories ATTN: SLCBR-SE-I Mr. Harry Rogers SLCBR-VL-V Dr. Paul Dietz Aberdeen Proving Ground, MD 21005-5066		 1 1
Commander U. S. Army Communications Electronics Command Electronics Warfare RSTA Center Ft. Monmouth, NJ 07703		1
AMSMI-RD,	Dr. Rhoades	1
AMSMI-RD-CS-R		5
AMSMI-RD-CS-T		1
AMSMI-RD-MG,	Mr. Jackson Mr. Pittman	5 1
AMSMI-RD-MG-IR,	Mr. Currie	1
AMSMI-RD-MG-OL,	Mr. Miller	1
AMSMI-RD-MG-ST,	Dr. Loomis	1
AMSMI-RD-MG-IP,	Mr. Duke	1
AMSMI-RD-MG-RF,	Dr. Emmons Mr. Christian Mr. Green Ms. Mobley Mr. Mullins Mrs. Read Mr. Sedenquist	1 1 1 10 1 1 1
AMSMI-RD-SS-HW,	Mr. Cole	1
AMSMI-RD-SS-SD,	Mr. Sanders	1

INITIAL DISTRIBUTION LIST (conc.)

		Copies
AMSMI-RD-ST-WF,	Mr. Lovelace	1
AMSMI-RD-WS,	Dr. Bennett	1
AMSMI-GC-IP,	Fred Bush	1
AMSMI-SW,	Mr. George	1
AMCPM-AT		1
AMCPM-ML-TM,	Mr. Crosswhite	1
SFAE-FS-I,	Mr. Clem	1
SFAE-FS-XBE,	Ms. Frazier	1